Investigation of the π Character of a C−C Bond with the Help of the Diamagnetic and Paramagnetic Spin−Orbit Term of the NMR Spin−Spin Coupling Constant

Jürgen Gräfenstein, Elfi Kraka, and Dieter Cremer*

Department of Theoretical Chemistry, Göteborg University, Reutersgatan 2, S-41320 Göteborg, Sweden

Received: January 5, 2004; In Final Form: February 26, 2004

The NMR spin−spin coupling constant (SSCC) ^1J(C−C) is a sensitive antenna for investigating the electronic structure in hyper- and π-conjugated hydrocarbons. The magnetic dipole field of the perturbed nucleus generates orbital currents, which are experienced by the responding nucleus, thus leading to the paramagnetic spin−orbit (PSO) coupling mechanism. The strength of the orbital currents depends on the availability of high-lying occupied and low-lying virtual orbitals with distinct p_π or p_σ character, the nodal properties of these orbitals, and the overlap between zeroth- and first-order orbitals. For C−C bonds in unsaturated hydrocarbons, the value of ^{1}PSO(C−C) depends on opposing effects such as the p_σ and the p_π character of the C−C bond (i.e., the degree of hybridization at the C atoms and the degree of π delocalization in the conjugated system). This dependence leads to the overall cubic behavior of the PSO term when given as a function of the C−C bond character and the strong scattering of PSO values for a given bond type. Under certain conditions, the degree of hybridization can be determined with the help of the PSO term. Also, the PSO term helps to distinguish hyperconjugation and π-conjugation effects. For a given C−C bond type with fixed or similar hybridization at the C atoms, the PSO term can be given as a function of the C−C bond order, thus representing a sensitive descriptor for the degree of π delocalization.

1. Introduction

The notion of chemical bonds and their properties (bond strength, bond order, σ vs π character) is crucial to the explanation of chemical phenomena.[1−7] Because the chemical bond is not observable, bond quantities can be defined only within a given model of the chemical bond rather than directly measured in an experiment.[7] Of course, one can assess bond properties indirectly from thermochemical or spectroscopic data, for example. However, these data provide only limited insight into the properties of the bond. For example, bond dissociation results not only in the breaking of a bond but also in the relaxation of the fragments.[8−10] Bond-stretching vibrations involve distortions in the whole molecule, not just in the bond under investigation.[8−10] Bond lengths do not reflect the fact that the bond may be bent and accordingly may be longer than the distance between the two bonded nuclei.[11] Quantities such as bond-stretching forces[9] and bond dipole moments,[9] however, cannot be measured directly but have to be derived within a given model.

Indirect NMR spin−spin coupling constants (SSCC) provide information on the electron structure along a specific bond or a chain of bonds connecting the coupling nuclei in the molecule.[12,13] Thus, they are of potential use in the experimental investigation of chemical bonds. There have been numerous attempts[14−21] to relate SSCCs ^1J(C−C) and ^1J(C−H) in hydrocarbons to the s character of the C−C and C−H bond orbitals (expressed in terms of localized molecular orbitals (LMOs)[22]), the C−C bond length, its bond order, or its π character. These attempts proved successful and corroborated the idea of SSCCs containing useful information on the chemical bond.

For an analysis of the σ or π character of a bond with the help of spin−spin coupling information, it is important to consider that the SSCC contains four different contributions, the so-called Ramsey terms:[23] they are related to different spin−spin coupling mechanisms and probe different parts of the electron density. The Fermi-contact (FC) term, which dominates the total SSCCs in many cases, depends on orbitals with distinct s character at the coupling nuclei. The paramagnetic spin−orbit (PSO) and spin−dipole (SD) terms, in contrast, require orbitals with non-s character at the coupling nuclei. The diamagnetic spin−orbit (DSO) term does not depend on the character of an orbital; however, it is normally rather small. Hence, an analysis of the π character of a bond should be based upon the PSO and the SD term.

In a previous paper,[24] we analyzed the relationship between the π-bond order of typical C−C bonds in unsaturated hydrocarbons and the sum of the noncontact (NC = PSO + DSO + SD $\approx$ PSO + SD) terms of ^1J(C−C), henceforth called ^{1}NC-(C−C).[24] It was found that there is a cubic dependence of ^{1}-NC(C−C) on the C−C bond order, which results from the PSO term. The SD term increases exponentially with the bond order, whereas the PSO term adopts small positive or negative values for C−C single bonds, negative values for C−C double bonds, and large, positive values for C−C triple bonds.[24] For the purpose of explaining the dependence of the PSO spin−spin coupling mechanism on the C−C multiple bond character, we analyzed the PSO term for the prototypical C−C single, double, and triple bonds and could show that the orbital currents induced by the PSO coupling mechanism change in a characteristic way with the bond character.[25]

This analysis of the PSO coupling mechanism clarified the cubic dependence of the PSO term on the C−C bond order and set the basis for using this term as a suitable parameter to describe the C−C bond. However, all attempts to establish

* Corresponding author. E-mail: cremer@theoc.gu.se.

10.1021/jp049954s CCC: $27.50
Published on Web 04/28/2004

SCHEME 1: Numbering of Atoms in Molecules 1−12

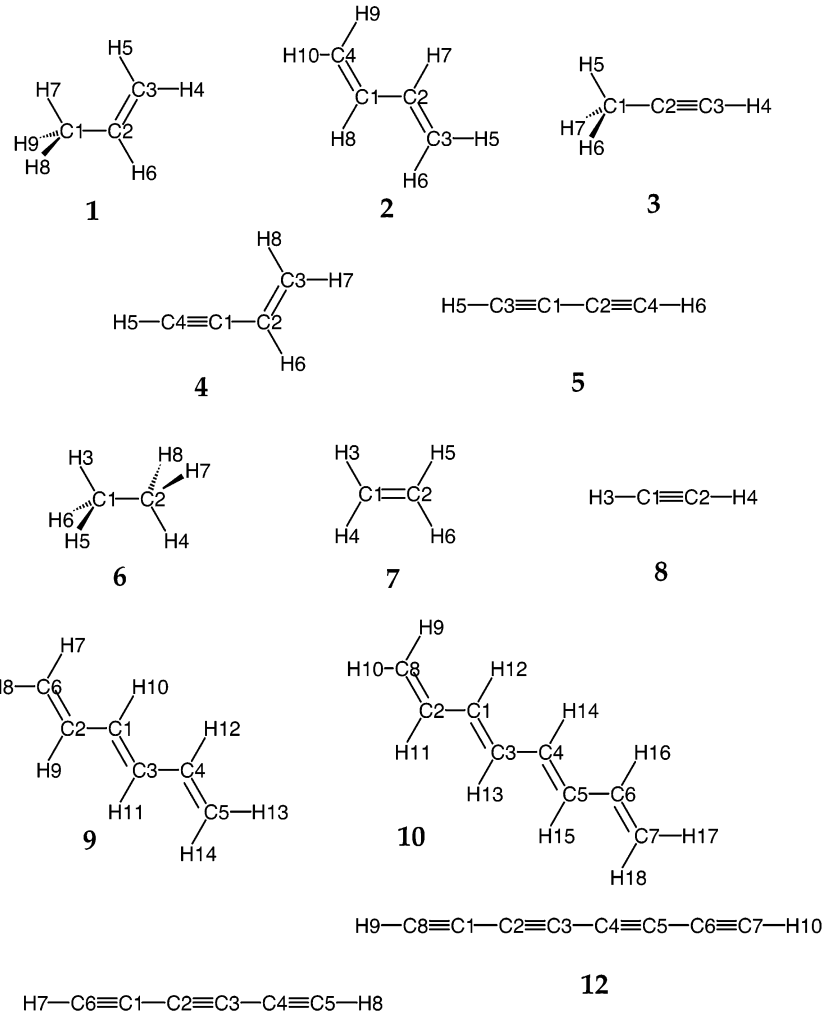

practically useful relationships between ^{1}PSO(C−C) and the π-bond order failed because of the strong scattering of data points in the case of formal single bonds in a number of conjugated or hyperconjugated hydrocarbons.[24] It seems that for the SSCC ^1J(C−C) of formal single bonds the PSO term behaves erratically and does not follow any rules, which is contrary to the systematic changes observed when increasing the C−C bond order by one unit.

In the present paper, we investigate the PSO coupling mechanism in hyperconjugated and π-conjugated hydrocarbons with C−C single bonds possessing partial π character: propene (**1**), *trans*-1,3-butadiene (**2**), methylacetylene (**3**), vinylacetylene (**4**), and 1,3-butadiyne (**5**). As suitable reference molecules, we use staggered ethane (**6**), ethylene (**7**), and acetylene (**8**, see Scheme 1). In addition, we will study selected long-range SSCCs of *trans*,*trans*-1,3,5-hexatriene (**9**), *trans*,*trans*,*trans*-1,3,5,7-octatetraene (**10**), 1,3,5-hexatriyne (**11**), and 1,3,5,7-octatetrayne (**12**) to determine the limits of long-range coupling. Molecules **1**−**12** span the manifold of different C−C single bonds as they occur in unsaturated hydrocarbons.

For the purpose of calculating SSCCs ^1J(C−C) and their four Ramsey terms for the molecules of Scheme 1, we use coupled perturbed density functional theory (CP-DFT) and the algorithm described previously by us.[26] The tools for analyzing the PSO coupling mechanism will be briefly discussed in section 2. Some background theory is summarized in the Appendix. In section 3, the relationship between the PSO coupling mechanism and the electronic structure of the investigated molecules is discussed. The goal of this discussion is to point out the role of the PSO term in specific and spin−spin coupling in general as suitable descriptors for the nature of chemical bonding and the electronic structure of a molecule.

2. Computational Tools for Analyzing the PSO Coupling Mechanism

The Ramsey theory of indirect spin−spin coupling[23] between two nuclei A and B is based on mixed perturbation theory with respect to the magnetic moments of the two coupling nuclei. Starting from the picture that nucleus B ("perturbed nucleus") induces both spin polarization and orbital currents in the electron system of the molecule, which in turn give rise to an extra magnetic field at nucleus A ("responding nucleus"), the SSCC can be represented as a sum of FC and SD terms (related to the spin polarization of the electron system) as well as PSO and DSO terms (related to the induced orbital currents in the electron system). The original Ramsey theory was formulated for many-body Schrödinger theory;[23] however, for the purpose of calculating SSCCs with DFT, it was recently reformulated within CP-DFT.[26,27] A brief review of the DFT formulation of the Ramsey theory is given in the Appendix.

In CP-DFT, the four Ramsey terms are represented as sums over contributions from the Kohn−Sham orbitals. (See the Appendix, eqs A1−A10). Hence, each Ramsey term can be decomposed into one- and two-orbital contributions as was shown recently.[28−30] In addition, the four Ramsey terms and their orbital contributions are graphically represented in terms of spin polarization and current density distributions. This proves most straightforward for the FC term:[28−30] The spin polarization density induced by the magnetic moment of the perturbed nucleus provides insight into the way the information is transmitted through the molecule, and via the sign and magnitude of the polarization at the responding nucleus, it allows us to determine the sign and magnitude of the FC term directly. Analogously, one can analyze the SD coupling mechanism in terms of spin polarization densities.[31] Such an analysis is more complicated than that for the FC term in two ways: First, the SD term is anisotropic, and one has to consider the components of the spin density for each orientation of the perturbed spin. Second, the SD term does not depend locally on the spin polarization distribution at the responding nucleus (as in the case of the FC term) but is a weighted integral of the whole spin polarization distribution, the weight function being given by the operator $\mathbf{h}_A^{SD}$ (Appendix, eq A8). It is therefore useful to consider not only the spin polarization distribution itself but also the so-called SD energy density distribution, which is the spin polarization distribution weighted by $\mathbf{h}_A^{SD}$.[31]

For the PSO and DSO terms, a local analysis can be accomplished with the help of the orbital current density distributions induced by the nuclear magnetic moment of the perturbed nucleus, for which we have coined the names PSO and DSO current density distributions:[25]

$$\mathbf{j}_{\mathbf{n}}^{(B),DSO}(\mathbf{r}) = -\left\{\frac{1}{m}\frac{4\epsilon_0\hbar^2}{e^3}\right\}\alpha^2\rho^{(0)}(\mathbf{r})\left(\mathbf{n}\times\frac{\mathbf{r}-\mathbf{R}_B}{|\mathbf{r}-\mathbf{R}_B|^3}\right), \quad (1a)$$

$$\mathbf{j}_{\mathbf{n}}^{(B),PSO}(\mathbf{r}) = 2\left\{\frac{\hbar}{m}\right\}\sum_k^{occ}[\phi_{k,\mathbf{n}}^{(B),PSO}(\mathbf{r})\,\nabla\phi_k^{(0)}(\mathbf{r}) - \phi_k^{(0)}(\mathbf{r})\,\nabla\phi_{k,\mathbf{n}}^{(B),PSO}(\mathbf{r})] \quad (1b)$$

n is the orientation vector of the nuclear spin moment, and $\rho^{(0)}(\mathbf{r}) = 2\sum_k^{occ}|\phi_k^{(0)}(\mathbf{r})|^2$ is the zeroth-order electron density. With these current densities, the component *nn* of the PSO and DSO terms can be written as

$$K_{AB,\mathbf{nn}}^{(X)} = \left\{\frac{1}{m}\frac{4\epsilon_0\hbar^2}{e^3}\right\}\alpha^2\int d^3r\,\mathbf{n}\left(\mathbf{j}_{\mathbf{n}}^{(B),X}(\mathbf{r})\times\frac{\mathbf{r}-\mathbf{R}_A}{|\mathbf{r}-\mathbf{R}_A|^3}\right) \quad (2)$$

with X = PSO, DSO. That is, each diagonal component of the PSO and DSO terms is represented as a weighted integral over the corresponding current density, where the weight factor is given by $\mathbf{h}_A^X$ (Appendix, eq A8) and the isotropic terms are found according to eq A10 of the Appendix.

Equations 1 and 2 suggest the partitioning of the PSO coupling mechanism into two steps: In the first step, the magnetic dipole field generated by perturbed nucleus B leads to an orbital current, which can be visualized by plotting $\mathbf{j}_{\mathbf{n}}^{(B),PSO}$ given in eq 1b in an appropriate way. This current is equivalent to a particle current in the electron system. In the second step, the orbital current generates a magnetic field at nucleus A that favors either a parallel (negative contribution) or an antiparallel orientation (positive contribution) of the spins at A and B. The operator $\mathbf{h}_A^{PSO} = \alpha^2\mathbf{l}_A r_A^{-3}$ ($\mathbf{l}_A = \mathbf{r}_A\times\nabla$ is the angular momentum operator) measures the angular momentum part of this particle current density with respect to A and weights it by $1/r_A^3$. This means that the operator $\mathbf{h}_A^{PSO}$ extracts those parts of the orbital current that form ring currents around A and weights these currents more strongly the closer they are to A. This weighting procedure converts the (vector) PSO current into the (scalar) PSO energy density distribution. The weighting with l_A means that orbital currents flowing radially to or from A will not contribute to the PSO energy density. Also, a linear current through the region of A will result in contributions to the PSO energy density, which cancel each other. Altogether, $\mathbf{h}_A^{PSO}$ measures the efficiency of the PSO current in generating a magnetic field at A.

Analogously, a DSO energy density can be introduced. In distinction to the three other terms, the DSO term depends on the unperturbed state of the molecule only and can be calculated as a weighted integral over the unperturbed total density. In most cases, the DSO term is small, mainly because of nearly complete cancellation between positive and negative contributions.

Strictly speaking, the PSO and DSO couplings have to be regarded as parts of one coupling mechanism. This becomes evident from the fact that, first, the separation between DSO and PSO term is not unambiguous but can be modified by the gauge dependence of the vector potential, and second, the PSO and DSO current densities usually do not fulfill the continuity equation one by one but only in their sum. Despite this, DSO and PSO terms describe different induction mechanisms. This can be seen most clearly for the case of atoms. The DSO term describes the induction of ring currents by Larmor precession. This effect is present for any type of orbital. The PSO term, in contrast, can be comprehended as a modification of existing ring currents by the magnetic moment. We consider a pair of (complex) orbitals $p_\pm$ in an atom that is fully occupied. (The PSO term is easiest to discuss for complex orbitals.) The p_+ and p_- electrons carry opposite ring currents that cancel each other exactly in the absence of a magnetic field. A magnetic perturbation influences the $p_\pm$ electrons in the opposite way. One of the two ring currents is increased, whereas the other is decreased, which results in a nonvanishing net ring current for the $p_\pm$ orbital pair.

Because $\mathbf{h}_B^{PSO} = \alpha^2 l_B r_B^{-3}$, only occupied and virtual orbitals contribute to the PSO term that have non-s character around B, which is in line with the case in which the PSO mechanism modifies existing orbital currents. Thus, PSO coupling occurs only for selected orbitals, where in most cases it outweighs the DSO coupling. In hydrocarbons, the PSO mechanism is connected to those orbitals with a strong contribution from p atomic orbitals. The selection rules depend, then, on the choice of either real or complex orbitals. For complex orbitals and the perturbed moment oriented in the *z* direction, only $p_+ \rightarrow p_+^*$ and $p_- \rightarrow p_-^*$ kinds of excitation contribute to the PSO mechanism. For real orbitals, in contrast, the corresponding transitions are $p_x \rightarrow p_y^*$ and $p_x \rightarrow p_y^*$. Applied to molecules, this notation means that excitations from occupied orbitals with strong $p_\pm$ or $p_{x,y}$ character to virtual orbitals again with strong $p_\pm$ or $p_{x,y}$ character play a dominant role.

For the formal single bonds in **1**−**8** (Scheme 1; the numbering is carried out in the way that the C−C bonds investigated are always C1−C2 and, in the case of larger systems, C3−C4), the isotropic average and diagonal components of the SSCC ^1J(C−C) and its PSO and DSO terms (besides FC and SD terms) are calculated using CP-DFT[26] and the hybrid functional B3LYP.[32,33] The (11s,7p,2s/6s,2p)/[7s,6p,2d/4s,2p] basis set[34,35] designed for the calculation of magnetic properties was used.

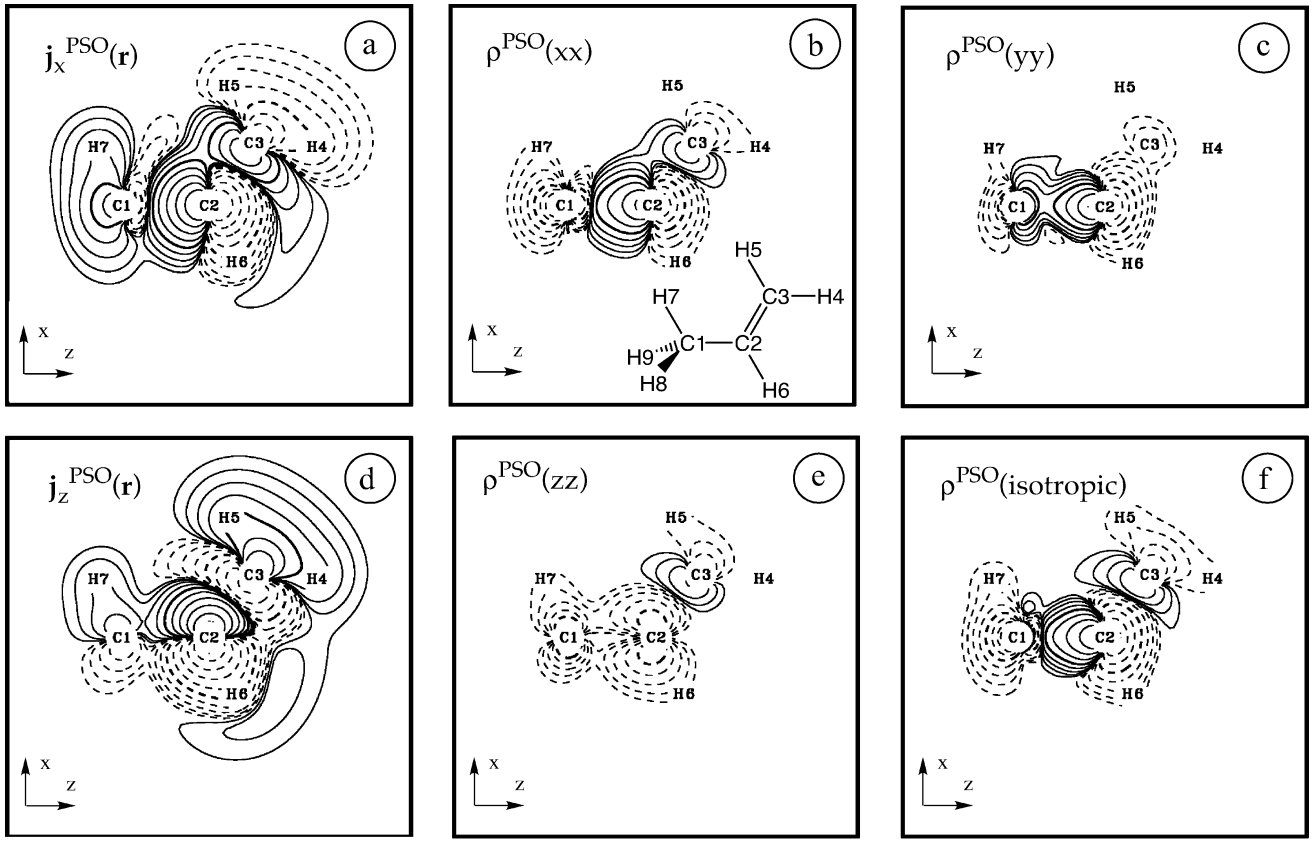

Figure 1. Contour-line diagrams of the PSO current densities and PSO energy densities for propene (**1**) in a plane containing the C atoms. C2 is the perturbed nucleus. The C1−C2 bond is oriented in the *z* direction; the C atoms are placed in the *xz* plane. For the PSO current densities, the component of the current perpendicular to the drawing plane is shown; solid (dashed) lines indicate a current out of (into) the plane. For the PSO energy densities, solid lines indicate positive contributions. CP-B3LYP/[7s,6p,2d/4s,2p] calculations were made. The contour levels are chosen in a geometric progression with a ratio of $100^{1/5} = 2.51188$. For the purpose of facilitating the comparison of magnitudes, contour lines belonging to levels ± 0.1 and ± 10 are given in bold. (a) Current density $\mathbf{j}_x^{PSO}(C2)$; (b) PSO energy density $\rho^{PSO}(xx)$ corresponding to $\mathbf{j}_x^{PSO}(C2)$; (c) PSO energy density $\rho^{PSO}(yy)$ corresponding to $\mathbf{j}_y^{PSO}$ (C2); (d) current density $\mathbf{j}_z^{PSO}$ (C2); (e) PSO energy density $\rho^{PSO}(zz)$ corresponding to $\mathbf{j}_z^{PSO}(C2)$; (f) isotropic PSO energy density distribution.

The SSCCs were calculated at the B3LYP/6-31G(d,p) geometries except for reference molecules **6**−**8**, where experimental geometries were used.[36−38]

Utilizing the calculated $|\phi_k^{(0)}\rangle$ and $|\vec{\phi}_k^{(B),PSO}\rangle$, we determined the current density distributions $\mathbf{j}_n^{(B),PSO}(\mathbf{r})$ and $\mathbf{j}_n^{(B),DSO}(\mathbf{r})$ for a given orientation of the spin moment of the perturbed nucleus and derived there from the PSO and DSO energy density distribution. The current densities $\mathbf{j}_x^{PSO}(\mathbf{r})$, $\mathbf{j}_y^{PSO}(\mathbf{r})$, and $\mathbf{j}_z^{PSO}(\mathbf{r})$ are represented as contour plots in a plane perpendicular to a component of the actual current. This representation gives a better account of the current distribution than streamlines or arrows in situations where the current densities vary by several orders of magnitude. Furthermore, streamlines are problematic when the current density is not divergence-free. The PSO and DSO energy densities, which are scalars, are also represented as contour plots. It should be noted that the plots of the current densities are specific to the perturbed nucleus only, whereas plots of the PSO density are specific to both the perturbed and the responding nuclei.

For all atoms, the formal single bond was aligned parallel to the *z* axis. The numbering of nuclei in molecules **1**−**8** is given in Scheme 1. The C skeleton of all molecules was placed into the *xz* plane so that the π system of the double bonds is oriented in the *y* direction. Nucleus C2 is always the perturbed nucleus; nucleus C1 is always the responding nucleus.

For the contour line representation of the isotropic average, the *xx*, *yy*, and *zz* components of the PSO (DSO) energy densities, and the *x*, *y*, and *z* components of the PSO (DSO) current densities, we have chosen contour lines in the form of a geometric progression using a multiplication factor of $100^{1/5} = 2.512$. In this way, the contour-level value of each fifth contour line has increased (decreased) by a factor of 100. For the purpose of simplifying the comparison of the diagrams shown in Figures 1−5, the contour lines with values 0.1 and 10 are given in bold. In all current density plots, solid (dashed) lines denote a current density out of (into) the drawing plane; the dotted lines are the zero contours.

For the purpose of identifying the main orbital contributions to the PSO (DSO) term, we used the J-OC-PSP (decomposition of *J* into *O*rbital *C*ontributions using *O*rbital *C*urrents and *P*artial *S*pin *P*olarization) developed recently.[28−30] This procedure leads for each Ramsey term to one- and two-orbital contributions, which we simplify in this work by (a) summing the two-orbital contributions into the one-orbital contributions and (b) also considering groups of orbitals in addition to single orbitals. The J-OC-PSP method is carried out for LMOs obtained with a Boys localization,[39] where core, σ, and π orbitals are separately localized for reasons described elsewhere.[28,29] We will base our analysis on the orbital contributions on LMOs; however, will discuss the PSO spin−spin coupling mechanism also in terms of canonical orbitals because the latter can be classified according to the symmetry of the molecule under investigation, which makes it easier to estimate the sign and magnitude of the matrix elements to be calculated for the SO terms. We note

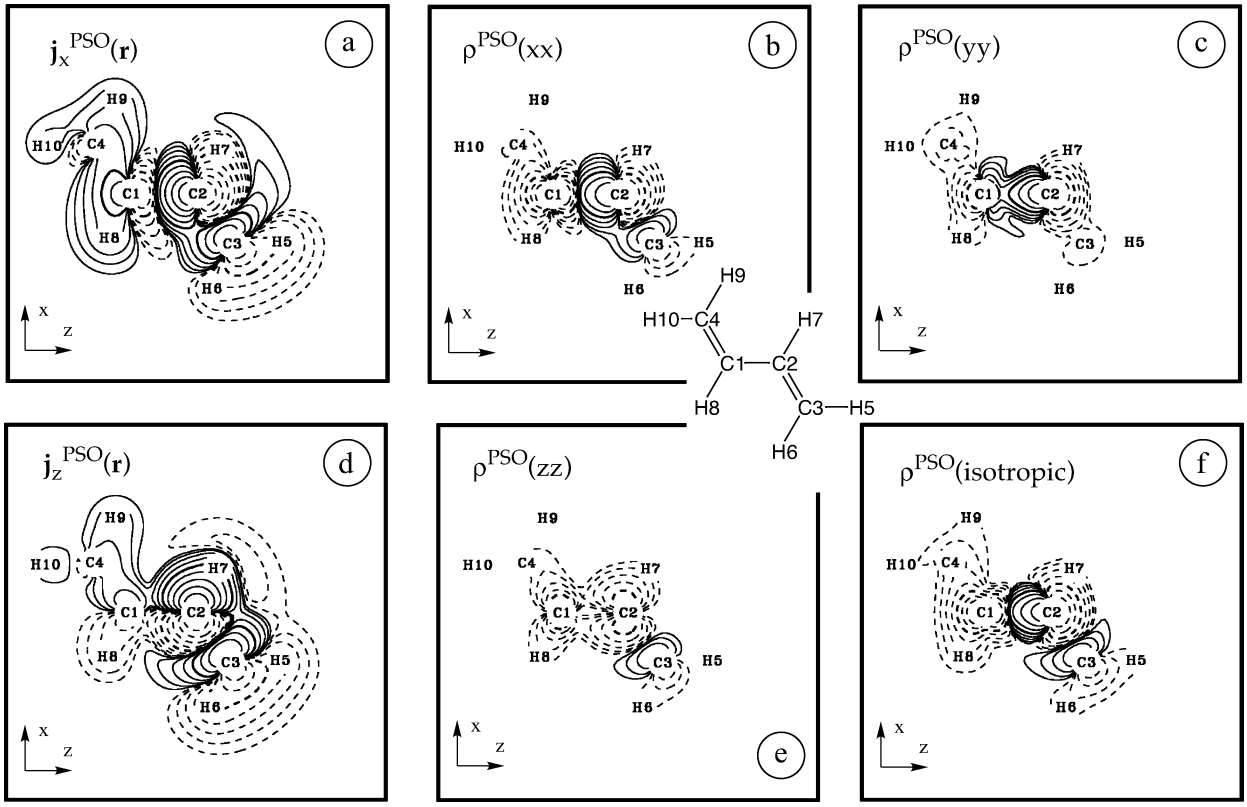

Figure 2. Contour-line diagrams of the PSO current densities and PSO energy densities for *trans*-1,3-butadiene (**2**) in a plane containing the C atoms. See Figure 1 for more details. (a) Current density $\mathbf{j}_x^{PSO}(C2)$; (b) PSO energy density $\rho^{PSO}(xx)$ corresponding to $\mathbf{j}_x^{PSO}(C2)$; (c) PSO energy density $\rho^{PSO}(yy)$ corresponding to $\mathbf{j}_y^{PSO}(C2)$; (d) current density $\mathbf{j}_z^{PSO}(C2)$; (e) PSO energy density $\rho^{PSO}(zz)$ corresponding to $\mathbf{j}_z^{PSO}(C2)$; (f) isotropic PSO energy density distribution.

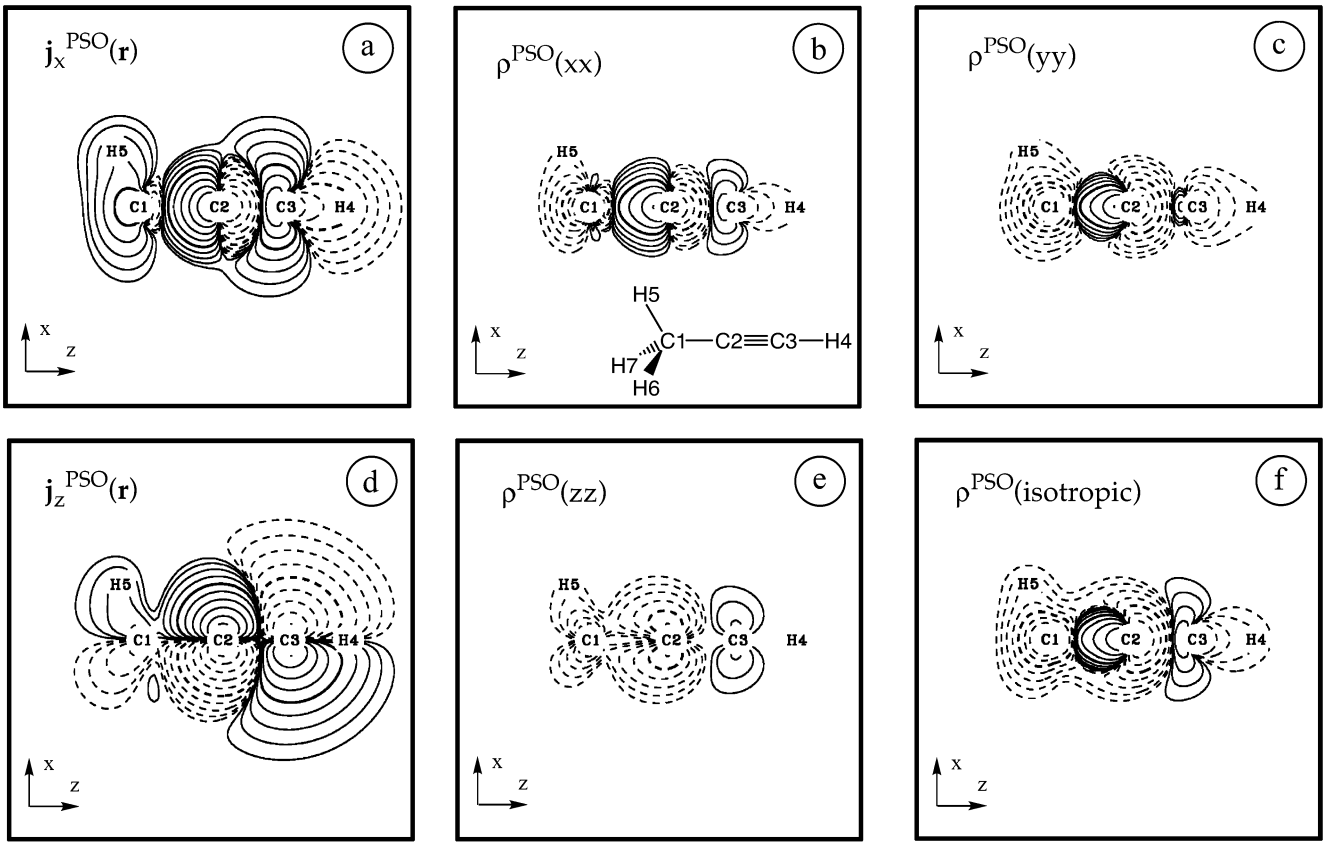

Figure 3. Contour-line diagrams of the PSO current densities and PSO energy densities for methylacetylene (**3**) in a plane containing the C atoms. See Figure 1 for more details. (a) Current density $\mathbf{j}_x^{PSO}(C2)$; (b) PSO energy density $\rho^{PSO}(xx)$ corresponding to $\mathbf{j}_x^{PSO}(C2)$; (c) PSO energy density $\rho^{PSO}(yy)$ corresponding to $\mathbf{j}_y^{PSO}(C2)$; (d) current density $\mathbf{j}_z^{PSO}(C2)$; (e) PSO energy density $\rho^{PSO}(zz)$ corresponding to $\mathbf{j}_z^{PSO}(C2)$; (f) isotropic PSO energy density distribution.

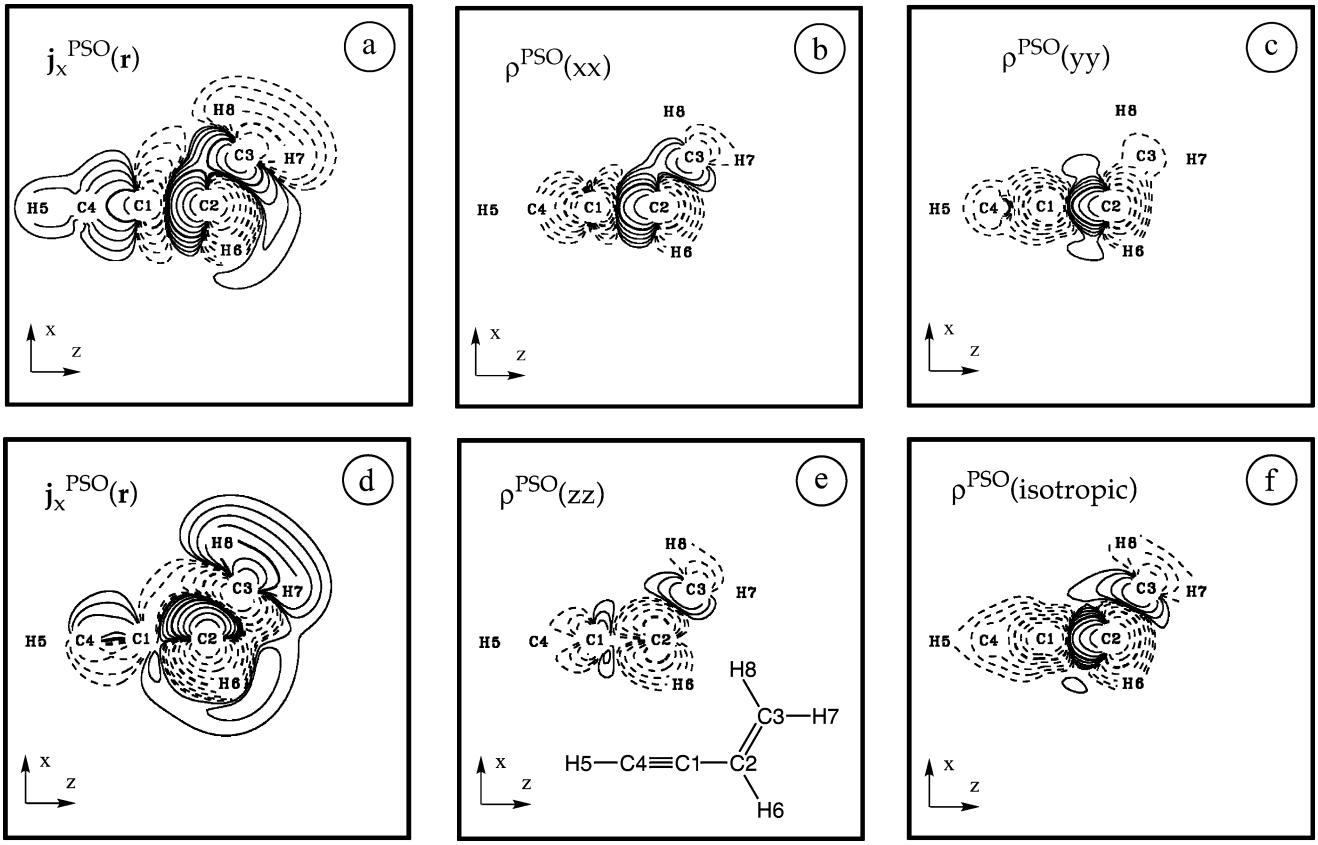

Figure 4. Contour-line diagrams of the PSO current densities and PSO energy densities for vinylacetylene (**4**) in a plane containing the C atoms. See Figure 1 for more details. (a) Current density $\mathbf{j}_x^{PSO}$(C2); (b) PSO energy density $\rho^{PSO}(xx)$ corresponding to $\mathbf{j}_x^{PSO}$(C2); (c) PSO energy density $\rho^{PSO}(yy)$ corresponding to $\mathbf{j}_y^{PSO}$(C2); (d) current density $\mathbf{j}_z^{PSO}$(C2); (e) PSO energy density $\rho^{PSO}(zz)$ corresponding to $\mathbf{j}_z^{PSO}$(C2); (f) isotropic PSO energy density distribution.

that no matter whether LMOs or canonical MOs are used for the analysis the results must be equivalent.

There are many definitions of the order of a C−C bond in a hydrocarbon, especially where the degree of π localization is concerned. As in the previous investigation,[24] we prefer a bond order that considers the total electron distribution rather than singling out just the π-density distribution. Therefore, we employed the AOM (atomic overlap matrix) bond order of Cioslowski and Mixon,[40] which is based on the virial partitioning method of Bader.[41] In addition, we calculated NBO (natural bond orbital) bond orders based on the NRT (natural resonance theory).[42,43] The π-bond order of a multiple C−C bond was calculated using Hückel, NRT, and AOM bond orders. All calculations were carried out with the ab initio program packages COLOGNE 2003[44] and Gaussian 98.[45]

3. Results and Discussion

In Table 1, calculated SSCCs ^1J(C−C) and their four Ramsey terms are listed for hydrocarbons **1**−**5** and reference molecules **6**−**8** (Scheme 1). Also given are experimental SSCCs[18,46] and the bond orders calculated with the AOM and NRT approaches. Table 2 shows the diagonal components for $^1J^{PSO}$ of the formal C−C bonds in **1**−**5** in comparison to the corresponding values for the C−C bonds in **6**−**8**. Calculated PSO current densities and PSO energy densities are graphically displayed in the form of contour line diagrams in Figures 1−5.

Calculated and measured SSCCs ^1J(C−C)[18,46] agree within 1 Hz in the case of C−C single bonds and within 5 Hz in the case of C−C double bonds. Larger deviations are found for the triple bond in acetylene (about 30 Hz), which decreases, however, by 10 Hz when vibrational corrections are included into the calculated ^1J(C−C) value[47] and by another 5 Hz when solvent effects are taken into account.[48] The calculated values are always larger than the measured values, which is an indirect indication of the well-known singlet−triplet instability problem, from which methods suffer that cannot provide sufficient nondynamic electron correlation for the calculation of the SSCC and, in particular, the calculation of the FC term. DFT with the approximate functionals used today has the advantage of including a large amount of unspecified nondynamic electron correlation,[49] which helps to improve the calculation of the FC term and the total SSCC. The limitations of this description become obvious with the increasing multiple bond character of the C−C bond and/or the reduced singlet−triplet splittings. (See ref 26 for a detailed discussion of this issue.) This is reflected by the eigenvalues of the stability matrix,[50] which are too small or even negative.

The NC terms of ^1J(C−C) are related to the C−C bond order by a cubic function as shown in Figure 6. The value of the NC term decreases from 1.2 Hz (C−C single bond of 6, Table 1) to −0.4 (C−C single bond with hyperconjugation in **1**), −1.5 (formal C−C single bond in the conjugated system of **2**), and −6.3 Hz (double bond in **7**), and then it increases again to 20 Hz (C−C triple bond in **8**). The cubic behavior of the NC term as a function of the p character or the bond order results from the PSO term, which in turn adopts this form from its components along and perpendicular (in the molecular plane) to the C−C bond, *zz* and *xx* (Table 2).

Although it is possible to obtain reasonable estimates of both the NC and the PSO term from the bond order, the usefulness

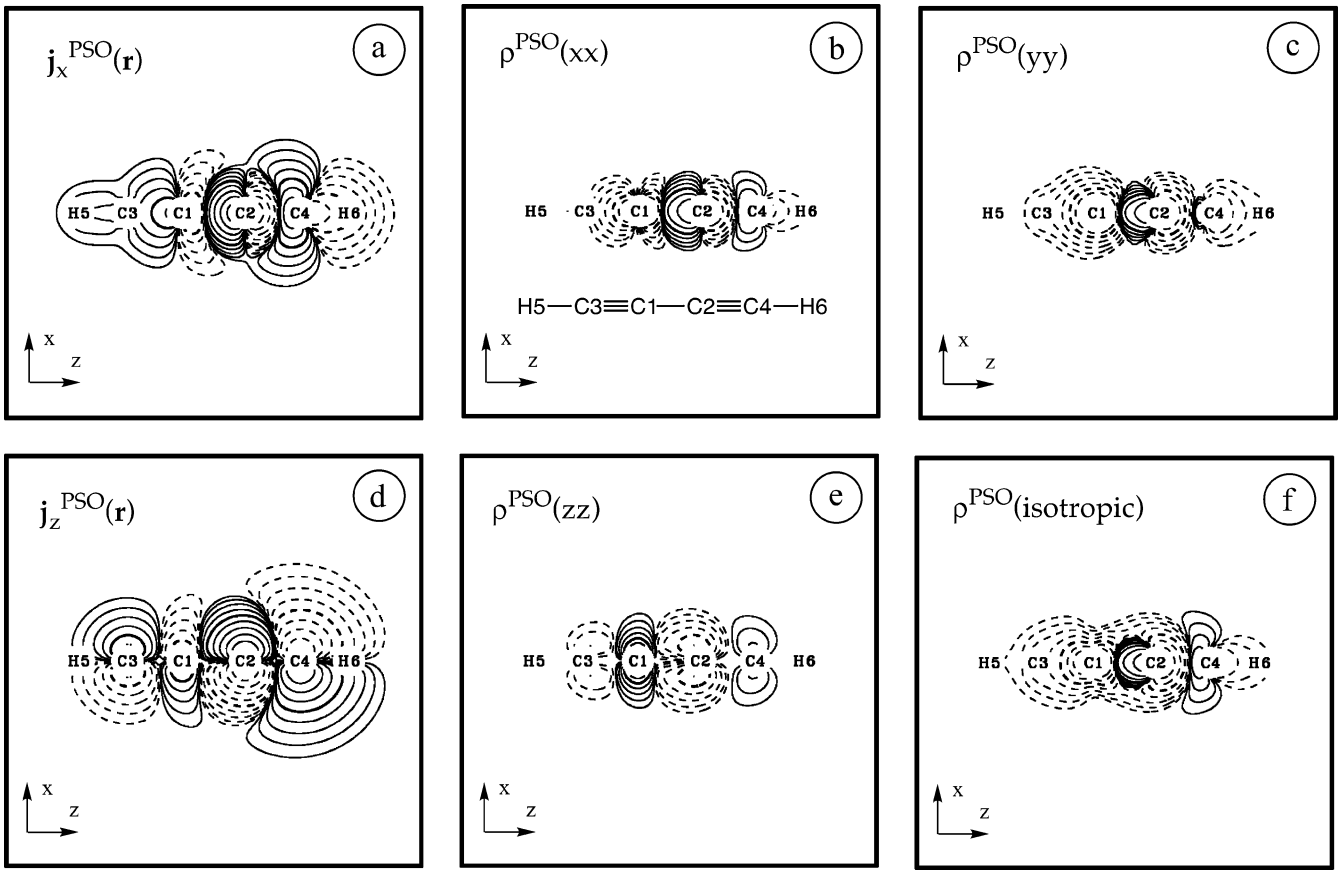

Figure 5. Contour-line diagrams of the PSO current densities and PSO energy densities for 1,3-butadiyne (**5**) in a plane containing the C atoms. See Figure 1 for more details. (a) Current density $\mathbf{j}_x^{PSO}$(C2); (b) PSO energy density $\rho^{PSO}(xx)$ corresponding to $\mathbf{j}_x^{PSO}$(C2); (c) PSO energy density $\rho^{PSO}(yy)$ corresponding to $\mathbf{j}_y^{PSO}$(C2); (d) current density $\mathbf{j}_z^{PSO}$(C2); (e) PSO energy density $\rho^{PSO}(zz)$ corresponding to $\mathbf{j}_z^{PSO}$(C2); (f) isotropic PSO energy density distribution.

TABLE 1: Ramsey Terms of *J*(C−C) for the C−C Single Bonds in 1−6 and the C−C Multiple Bonds in 7 and 8[a]

molecule	FC	DSO	PSO	SD	$^1J^A$(C−C)	^1J(C−C)	^1J(C−C) exp	NRT	AOM
1	42.54	0.16	−1.34	0.75	−0.43	42.11	41.9	1.024	1.061
2	56.72	0.21	−3.02	1.32	−1.49	55.23	53.7	1.061	1.114
3	73.08	0.15	−1.70	0.42	−1.13	71.95	67.4	1.039	1.095
4	95.81	0.20	−2.74	0.94	−1.59	94.21	86.7	1.066	1.145
5	172.04	0.22	−2.66	1.62	−0.82	171.22	153.4	1.115	1.237
6	32.77	0.13	0.01	1.08	1.22	34.00	34.5	1.024	1.035
7	76.88	0.08	−10.28	3.94	−6.26	70.62	67.5	1.947	2.023
8	181.67	0.07	8.38	11.60	20.05	201.73	169.7	2.994	2.902

[a] All contributions are given in hertz. SSCC calculations were made at the B3LYP/[7s,6p,2d/4s,2p] level of theory. B3LYP/6−31G(d,p) geometries were used for **1**−**5**; experimental geometries were used for **6**−**8**. For the numbering of molecules, see Scheme 1. $^1J^A$(C−C) is the sum of the noncontact terms. Experimental values for **1**−**5** are from ref 18, and those for **6**−**8** are from ref 46.

TABLE 2: Isotropic and Diagonal PSO Components of ^1J(C−C) for the C−C Single Bonds in 1−6 and the C−C Multiple Bonds in 7 and 8[a]

orientation	**1**	**2**	**3**	**4**	**5**	**6**	**7**	**8**
xx	−2.58	−7.00	−1.58	−5.37	−4.41	0.79	−26.63	−14.07
yy	0.56	0.15	−1.58	−1.43	−4.41	0.79	−0.04	−14.07
zz	−2.00	−2.20	−1.70	−1.42	0.85	−1.54	−4.18	53.27
isotropic	−1.34	−3.02	−1.93	−2.74	−2.66	0.01	−10.28	8.38

[a] All contributions are given in hertz. SSCC calculations were made at the B3LYP/[7s,6p,2d/4s,2p] level of theory. For the numbering of molecules, see Scheme 1. The single bond C1−C2 is oriented in the *z* direction, the *y* direction is given by the π orbitals, and the planar part of the molecule is in the *xz* plane.

of such an approach has to be questioned in view of the large scattering of the NC terms for the formal single bonds of molecules **1**−**5** (inset of Figure 6). As can also be seen from Figure 6, it is the PSO term that is responsible for the scattering of NC terms. Therefore, it is the goal of this work to gain a better understanding of the dependence of the PSO term of ^1J(C−C) on the π character of formal C−C single bonds. For this purpose, we discuss first the isotropic PSO term and the PSO components of ^1J(C1−C2) in molecules **7** and **8**.

C−C Reference Bonds. We start with molecule **8** because the higher symmetry facilitates the analysis. Figure 7a indicates schematically the ring currents in *xy* planes passing through C1 and C2 of **8**. These are induced by the spin moment of nucleus C2 oriented along the *z* axis and thus leading to ^{1}PSO(*zz*). The ring currents are in opposite directions around C1 (clockwise if viewed from C2) and C2 (counterclockwise, Figure 7a). They are mainly due to excitations from the $\pi_{x,y}$ orbitals into the corresponding $\pi^*_{y,x}$ orbitals, where the latter are responsible for the nodal surface between the two ring currents (Figure 7a,

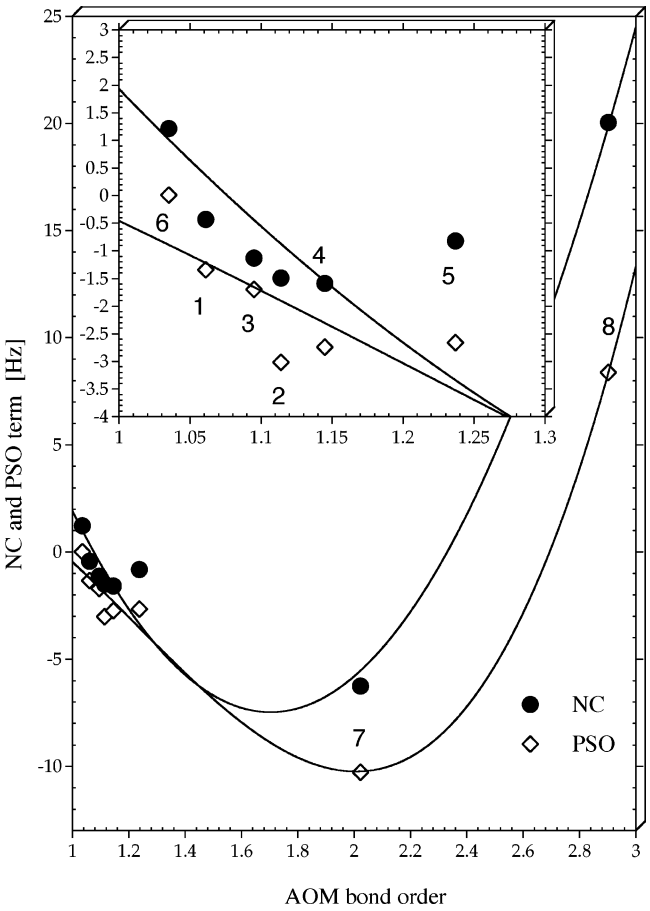

Figure 6. Functional dependence of the calculated NC term $^1J^A$(C−C) (●) and $^1J^{PSO}$(C−C) (◊) on the bond order AOM(C−C). All SSCC terms were calculated at the CP-DFT/B3LYP/[7s,6p,2d/4s,2p] level, and bond orders were calculated at the B3LYP/6-31G(d,p) level of theory. The inset gives NC and PSO values for formal C−C single bonds in π-conjugated and hyperconjugated molecules. Molecules are numbered according to Scheme 1. The following functional relationships were determined in ref 24 (x... bond order): PSO $= -2.20x^3 + 29.07x^2 - 81.10x + 55.05$ ($r^2 = 0.971$), NC $= -2.25x^3 + 31.72x^2 - 84.61x + 56.57$ ($r^2 = 0.977$).

middle). Because zeroth- and first-order orbitals overlap efficiently in this case and because the excitation energy is relatively small, the induced paramagnetic ring current is relatively strong. The opposite directions of the paramagnetic ring currents can also be viewed as resulting from the form of the magnetic dipole field μ (Figure 7a): In the π space of C2, this field points preferentially in the direction C1 → C2; however, in the π space of C1, this field points in the opposite direction (dashed arrows in Figure 7a). The ring current around C1 makes a positive contribution, and the ring current around C2 makes a negative contribution to the PSO energy density. Considering that C1 is the responding nucleus and that the PSO currents are weighted with $1/\mathbf{r}_A^3$, the positive contribution is larger than the negative one, where this effect is enlarged by the rotational symmetry of the PSO_{zz} density distribution around the z axis (^{1}PSO(zz) = 53.3 Hz, Table 2).

Figure 7b schematically presents the orbital currents for **8** in the *xz* plane with the perturbed nuclear moment oriented in the *y* direction. There are two ring currents with equal orientation: one around C2 and one around C1. The current density $\mathbf{j}_y^{PSO}(\mathbf{r})$ can be given only in the *yz* plane, not in the *xz* plane. However, for **8**, $\mathbf{j}_y^{PSO}(\mathbf{r})$ is equivalent to $\mathbf{j}_x^{PSO}(\mathbf{r})$, which can be shown in the *xz* plane (Figure 7c, middle). The latter has several nodal surfaces, which can be explained from the excitations σ_z(C−C) → π_y^*(C−C) and π_y(C−C) → σ_z^*(C−C). Because one of these orbitals (either π_y^* or σ_z^*) has a nodal surface perpendicular to the C1−C2 bond and the σ_z or σ_z^* orbitals possess an additional nodal surface through the C nuclei, the nodal structure of the current density $\mathbf{j}_x^{PSO} = \mathbf{j}_y^{PSO}$ (Figure 7c, middle) is obtained. The PSO(yy) energy density (middle of Figure 7b) is uniformly negative around C1 (apart from a rather small positive region at C2). This is confirmed by the *xx* distribution in the *xz* plane (Figure 7c, right) The value of $yy = xx$ is equal to −14 Hz (Table 2). Considering that the energy for the excitation π(C−C) → π^*(C−C) is much smaller than for the excitation σ(C−C) → π^*(C−C), it is easy to predict that the PSO(zz) component dominates and that a positive PSO value results (8.4 Hz, Table 2). This can also be derived from the orientation-averaged PSO energy density for **8** (Figure 7b, right), which gives a superposition of the features of the $\rho^{PSO}(zz)$, $\rho^{PSO}(yy)$, and $\rho^{PSO}(xx)$ energy density distributions. The toroidal region with positive contributions around C1 from the zz term dominates, although it is partially compensated by the negative contributions arising from the xx and yy terms. In this connection, it is important to note that the PSO energy density close to responding nucleus C1 dominates the PSO term.

In the case of **7** (Figure 8), the PSO ring current j_z around the molecular axis is considerably weaker (Figure 8a), and contrary to that in **8**, it is uniformly oriented (counterclockwise when viewed from C2) throughout the molecule. The excitations involved are of the π_y → pseudo-π_x^* or pseudo-π_x → π_y^* type; these require a larger energy than the $\pi_{x,y}$ → $\pi_{y,x}^*$ excitations and accordingly lead to a weaker PSO current $\mathbf{j}(z)$ as reflected by the current density $\mathbf{j}_z^{PSO}(\mathbf{r})$ (Figure 8a, middle). Because the pseudo-π_x^* orbital is C−C bonding, there is no nodal plane through the center of the C−C bond (the same result is obtained for the pseudo-π_x → π_y^* excitation because both occupied and virtual orbitals possess a nodal surface through the C1−C2 bond in this case), which of course implies that the local contributions to the currents around C2 and around C1 cancel each other, partially leading to a smaller current density at C1 (Figure 8a). The PSO energy density $\rho^{PSO}(zz)$ is negative throughout, leading to a PSO(zz) value of −4.2 Hz.

The perturbation in the *y* direction generates a ring current around C2 of **7** (Figure 8b), but contrary to **8** (Figure 7b), there is no second ring current around C1 in the *xz* plane. The main contribution to the ring current results from the excitation σ_z(C−C) → pseudo-π_x^*(H_2C-CH_2). (The excitation pseudo-π_x-(H_2C-CH_2) → σ^*(C−C) plays a smaller role because of the high energy of the σ_z^*(C−C) orbital.) These orbitals are both C−C bonding, which explains that there is just one ring current around C2 (rather than two—one around C2 and one around C1—as in the case of **8**; compare Figures 7b and 8b) in the *xz* plane. Because we use the *xz* plane as drawing plane, we cannot represent the perpendicular current density. However, in the *yz* plane, this is uniformly positive around C1. Neither the ring current around C2 nor the uniform current around C1 generates a sizable magnetic field at C1, which explains the small value of the *yy* component of the PSO term. Positive and negative energy densities $\rho^{PSO}(yy)$ cancel each other out, and a value close to zero results for this component.

For the perturbed moment oriented in the *x* direction, the induced currents are in the *yz* plane. The current density in the *xz* plane (Figure 8c, middle) resembles that displayed for **8** in Figure 7c, as confirmed by the PSO density (Figure 8c, right) shown for the *xz* plane. The main contribution results from the excitation σ_z(C−C) → π_y^*, which because of the nodal struc-

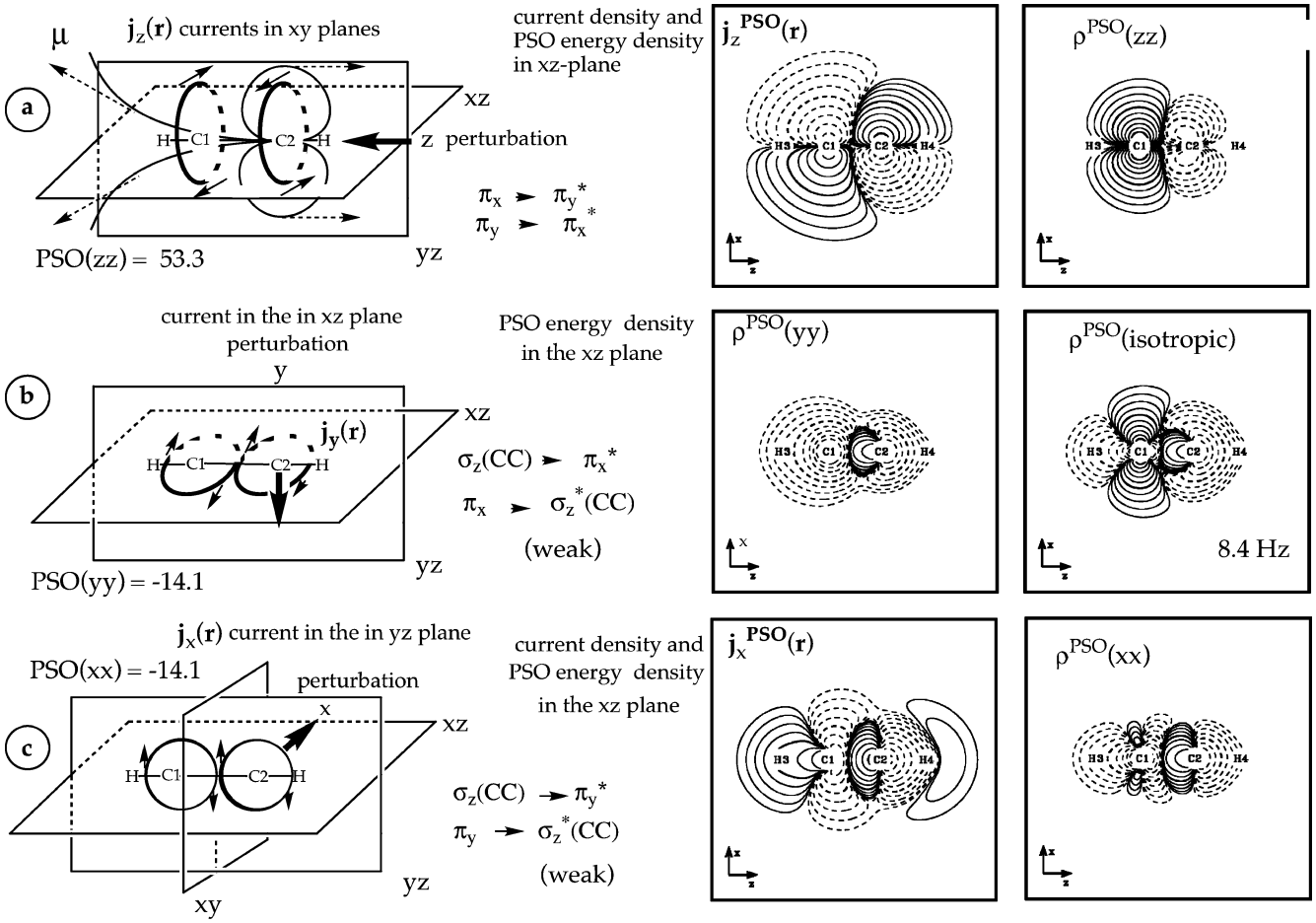

Figure 7. Description of the PSO components of ^1J(C−C) in acetylene (**8**). (a, left) Schematic presentation of the orientation and direction of the orbital currents $\mathbf{j}_z(\mathbf{r})$ (bold circles with small arrows) in the *xy* planes containing perturbed nucleus C2 and responding nucleus C1 for a perturbation in the *z* direction (bold arrow). The direction of the magnetic dipole field μ is indicated by dashed arrows; the field lines are indicated by normal lines. The dominating electron excitations and the $\rho^{PSO}(zz)$ value (in Hz) are given. (middle) Contour-line diagram of the current density distribution $\mathbf{j}_z^{PSO}(\mathbf{r})$ in the *xz* plane. Solid (dashed) lines indicate a current out of (into) the plane. right: PSO energy density distribution $\rho^{PSO}(zz)$ corresponding to $\mathbf{j}_z^{PSO}(\mathbf{r})$ in the *xz* plane. Solid lines denote a positive PSO energy density. (b) Schematic presentation of the orientation and direction of the orbital currents $\mathbf{j}_y(\mathbf{r})$ (bold circles with small arrows) in the *xz* plane containing perturbed nucleus C2 and responding nucleus C1 for a perturbation in the *y* direction (bold arrow). The dominating electron excitations and the $\rho^{PSO}(yy)$ value (in Hz) are given. (middle) PSO energy density distribution $\rho^{PSO}(yy)$ corresponding to $\mathbf{j}_y^{PSO}(\mathbf{r})$ (not shown) in the *xz* plane. Solid lines denote a positive PSO energy density. (right) Isotropic PSO energy density distribution ρ^{PSO}(isotropic). (c, left) Schematic presentation of the orientation and direction of the orbital currents $\mathbf{j}_x(\mathbf{r})$ (bold circles with small arrows) in the *yz* plane containing perturbed nucleus C2 and responding nucleus C1 for a perturbation in the *x* direction (bold arrow). The dominating electron excitations and the $\rho^{PSO}(xx)$ value (in Hz) are given. (middle) Contour-line diagram of the current density distribution $\mathbf{j}_x^{PSO}(\mathbf{r})$ in the *xz* plane. Solid (dashed) lines indicate a current out of (into) the plane. (right) PSO energy density distribution $\rho^{PSO}(xx)$ corresponding to $\mathbf{j}_x^{PSO}(\mathbf{r})$ in the *xz* plane. Solid lines denote a positive PSO energy density.

ture of these orbitals (σ_z(C−C): nodal surfaces through C1 and C2 perpendicular to the C−C bond axis; π_y^*: one perpendicular nodal surface through the midpoint of the C−C bond) leads to the current density pattern $\mathbf{j}_x^{PSO}(\mathbf{r})$ displayed in Figure 8c (middle). There is a pair of ring currents around C1 and C2 in the *yz* plane. The ring currents cancel each other in the *xy* plane bisecting the C−C bond. The resulting PSO energy density $\rho^{PSO}(xx)$ is dominantly negative (Figure 8c, right), causing a large negative value: PSO(*xx*) = −26.6 Hz (Table 2). The larger value for **7** compared to that for **8** results from the stronger p_z character of the σ_z(C−C) orbital in **7** (sp^2 rather than sp). Also, the larger electronegativity of an sp-hybridized C atom implies that the σ_z and π orbitals are lower in energy and the π^* orbital is higher in energy in **8** than in **7**, thus leading to higher excitation energies in the former case. The orientation-averaged PSO density (Figure 8b, right) resembles that of the *xx* component, which outweighs the other diagonal elements by a factor of more than 6.

In Figure 9, PSO current densities and PSO energy densities for ^1J(C−C) of **6** are shown. There are similarities to the corresponding quantities of both **8** and **7** (Figures 7 and 8). The PSO current density $\mathbf{j}_z^{PSO}(\mathbf{r})$ and the PSO energy density $\rho^{PSO}(zz)$ (Figure 9d and e) resemble those of **7** rather than those of **8**, which is due to the fact that two of the three dominating pseudo-$\pi_{x,y} \rightarrow$ pseudo-$\pi_{x,y}^*$ excitations lead to a uniform ring current around the C−C axis (no perpendicular nodal surface through the middle of the C−C bond). Because the excitation energies are larger for **6** than for **7**, the PSO(*zz*) component is just −1.5 Hz. The excitations σ_z(C−C) → pseudo-$\pi_{x,y}^*$ and pseudo-$\pi_{x,y} \rightarrow \sigma_z^*$(C−C) cause ring currents j_y and j_x in the *xz* and *yz* planes, which because of the nodal pattern of the participating orbitals enclose both C2 and C1 (similar to the case of j_y for **7**, Figure 8b). The corresponding PSO energy densities $\rho^{PSO}(xx)$ (Figure 9b) and $\rho^{PSO}(yy)$ (Figure 9c) suggest a balance between negative and positive contributions in line

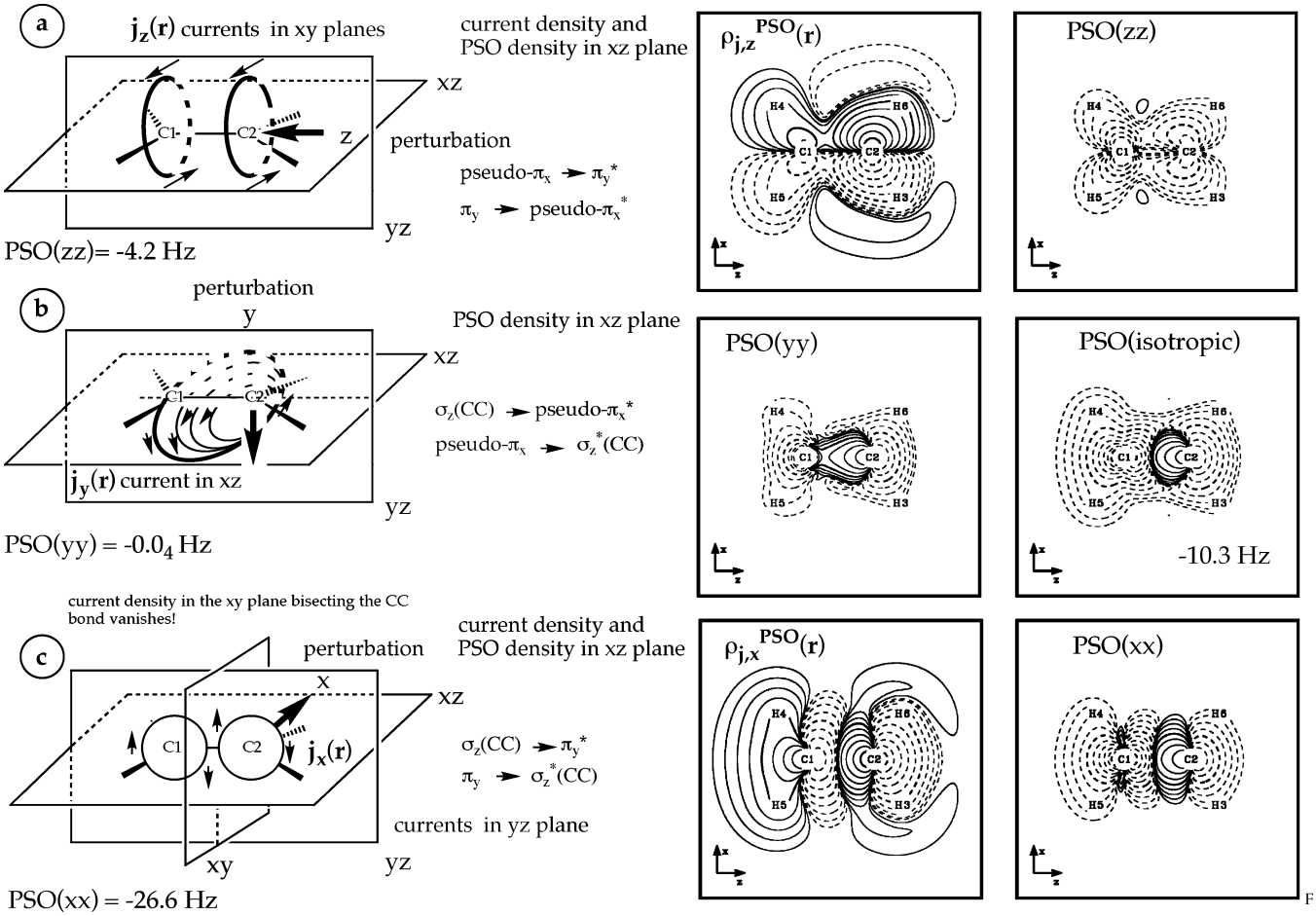

Figure 8. Description of the PSO components of ^1J(C−C) in ethylene (**7**). (a, left) Schematic presentation of the orientation and direction of the orbital currents $\mathbf{j}_z(\mathbf{r})$. (middle) Contour-line diagram of the current density distribution $\mathbf{j}_z^{PSO}(\mathbf{r})$. (right) PSO energy density distribution $\rho^{PSO}(zz)$ corresponding to $\mathbf{j}_z^{PSO}(\mathbf{r})$. (b) Schematic presentation of the orientation and direction of the orbital currents $\mathbf{j}_y(\mathbf{r})$. (middle) PSO energy density distribution $\rho^{PSO}(yy)$ corresponding to $\mathbf{j}_y^{PSO}(\mathbf{r})$ (not shown). (right) Isotropic PSO energy density distribution ρ^{PSO}(isotropic). (c, left) Schematic presentation of the orientation and direction of the orbital currents $\mathbf{j}_x(\mathbf{r})$. (middle) Contour line diagram of the current density distribution $\mathbf{j}_x^{PSO}(\mathbf{r})$. (right) PSO energy density distribution $\rho^{PSO}(xx)$ corresponding to $\mathbf{j}_x^{PSO}(\mathbf{r})$.

with the small positive values of the *xx* and *yy* components of the PSO term of 0.8 Hz (Table 2).

Formal C−C Single Bonds in Hyper- or π-Conjugated Systems. The calculated isotropic PSO values for the SSCC ^1J(C1−C2) in molecules **1**−**5** (Table 2) seem to reflect the partial π character of these bonds insofar as all values are negative; however, they are closer to the value of **6** than they are to the value of **7**. The overall pattern of the total PSO energy density (Figures 1f to 5f) resembles more that of **7**. (There is a nodal surface perpendicular to the C−C bond either through the midpoint or shifted toward C1.) This can be traced back to the $\rho^{PSO}(xx)$ energy density (Figures 1b−5b), which has in the C1−C2 bond region a pattern comparable to that of **7**.

Whereas the $\rho^{PSO}(xx)$ component and the corresponding energy density behave regularly, there are some irregularities for the *yy* and *zz* components, which can be both positive and negative (Table 2). The $\rho^{PSO}(yy)$ energy densities of **1** and **2** resemble that of **6**, which is confirmed by the fact that the calculated $\rho^{PSO}(yy)$ components are positive (0.56 and 0.15 Hz, Table 2). The energy densities $\rho^{PSO}(yy)$ of **3**−**5** are comparable to that of **8**, which is due to the neighboring triple bond. The values of the PSO(*yy*) components (−1.6, −1.4, −4.4 Hz; Table 2) are, however, closer to the value of ethylene (0 Hz) than to the value of acetylene (−14.1 Hz).

The $\rho^{PSO}(zz)$ energy densities of **1**−**4** are similar to that of **6** (and **7**; compare Figures 1d−4d and 1e−4e with 8a, middle and right). Only in the case of **5** there is a clear resemblance of the PSO(*zz*) current density and energy density distribution (Figure 5d and e) to the corresponding quantities for **8** (Figure 7a). The *zz* component is, however, just 0.85 Hz (contrary to 53.3 Hz in the case of **8**) because of a stronger cancellation of positive energy densities by negative energy densities (Figure 5e).

The analysis of the PSO term is facilitated by a JOC−PSP decomposition of the total PSO term into orbital contributions.[28,29] Table 3 lists the orbital contributions to the Ramsey terms of the SSCC ^1J(C1−C2) of **2** in terms of Boys LMOs. The orbital contributions in Tables 3 and 4 have been given in such a way that all two-orbital contributions are summed into the one-orbital term of that orbital that directly interacts with the responding nucleus (i.e., the contributions in Tables 3 and 4 refer to an explicit choice of perturbed and responding nucleus). By this convention, the orbital contributions are directly comparable with the Ramsey density plots. One sees that the dominating contribution to the total SSCC arises from the FC part of the σ(C1−C2) orbital and the σ orbitals of the adjacent bonds. Compared to the FC term, the PSO part is relatively small but still important when calculating ^1J(C1−C2). Again, the σ(C1−C2) orbital contribution dominates, but there are also smaller contributions from the π orbitals at the neighboring bonds (0.4, 0.1 Hz). We will therefore restrict the analysis of the PSO orbital contributions to these two groups

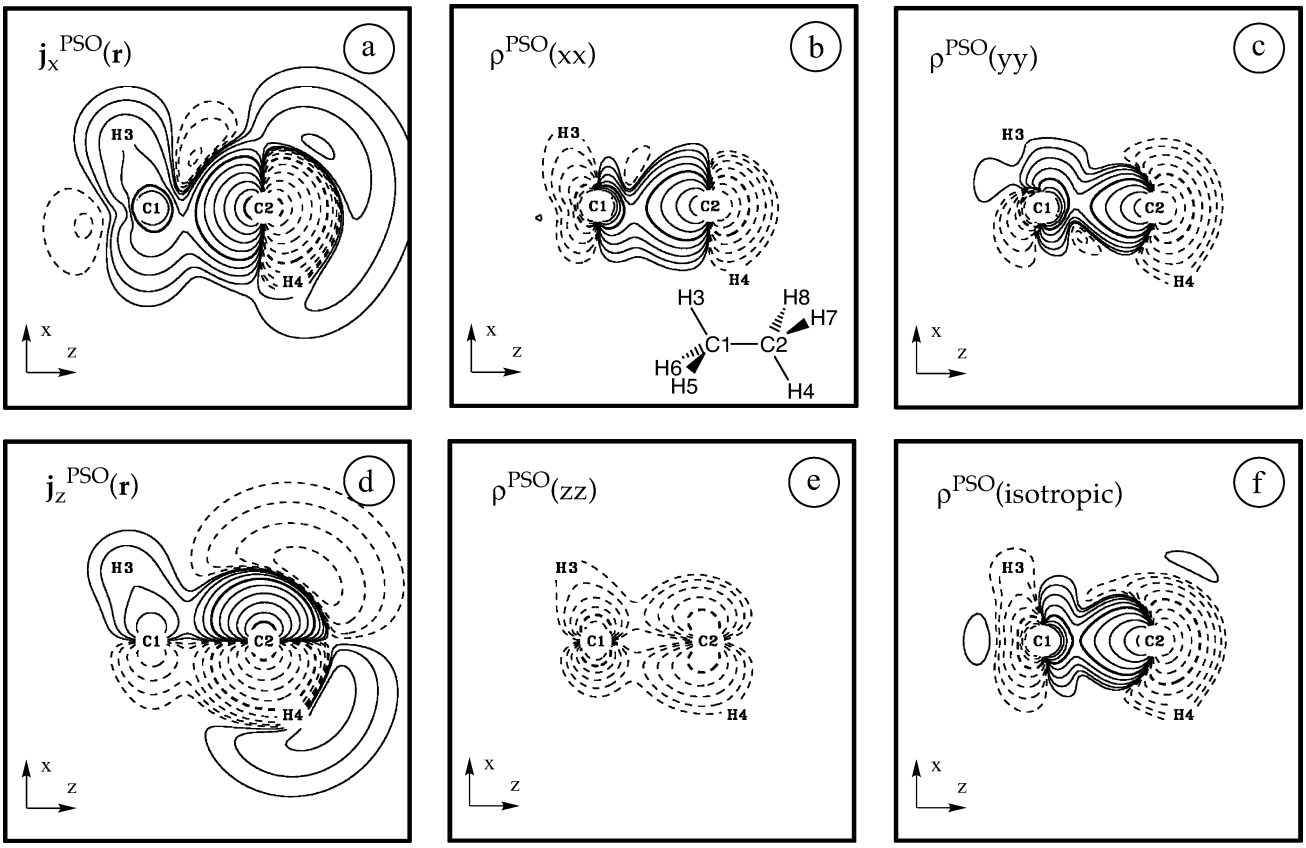

Figure 9. Contour-line diagrams of the PSO current densities and PSO energy densities for staggered ethane (**6**) in a plane containing the C atoms. See Figure 1 for more details. (a) Current density $\mathbf{j}_x^{PSO}(C2)$; (b) PSO energy density $\rho^{PSO}(xx)$ corresponding to $\mathbf{j}_x^{PSO}(C2)$; (c) PSO energy density $\rho^{PSO}(yy)$ corresponding to $\mathbf{j}_y^{PSO}(C2)$; (d) current density $\mathbf{j}_z^{PSO}(C2)$; (e) PSO energy density $\rho^{PSO}(zz)$ corresponding to $\mathbf{j}_z^{PSO}(C2)$; (f) isotropic PSO energy density distribution.

TABLE 3: Orbital Contributions to ^1J(C1−C2) in 1,3-Butadiyne[a]

orbital		PSO	DSO	FC	SD
1s	C1	0.00	0.00	−3.84	0.01
	C2	0.00	0.00	−0.10	0.00
	C3	−0.03	0.03	0.00	0.00
	C4	−0.03	0.03	0.00	0.00
bd σ	C1−C2	−2.12	−0.16	251.41	−0.06
ob σ	C1−C3	−0.04	0.05	−44.62	−0.05
	C2−C4	0.11	0.05	−27.08	−0.02
	C3−H5	−0.02	0.01	−2.34	0.00
	C4−H6	−0.03	0.01	−1.58	0.00
ob π	C1−C3	0.11	0.05	0.00	0.83
	C2−C4	−0.36	0.05	0.00	0.04

[a] All contributions are given in hertz. SSCC calculations were made at the B3LYP/[7s,6p,2d/4s,2p] level of theory. For atom numbering, see Scheme 1. The following orbital notations have been used: bd σ is the σ LMO of the investigated bond; ob σ and ob π are the σ and π LMOs of neighboring bonds, respectively. C2 is the perturbed and C1 is the responding nucleus.

of orbitals. Table 4 gives the contributions of the σ(C1−C2) orbitals as well as the π and pseudo-π orbitals to the PSO and DSO terms of SSCCs ^1J(C1−C2) in molecules **1**−**5**. Both the isotropic averages and the diagonal components of each orbital contribution are listed. Even though we focus our discussion on the PSO terms, the DSO terms are included to confirm that, despite the negligible contribution of the isotropic DSO term, individual contributions may be sizable.

Because there seems to be a systematic variation of the *xx* term, which depends on the C1−C2 bond character (Table 2), we pay special attention to this term by comparing Figures 1a to 5a and 1b to 5b in connection with the corresponding orbital contributions (Table 4). For all molecules, the ring current around C2 (perturbation in the *x* direction) is larger both in spatial extent and in its maximal amplitude than that around C1. The extent of the ring current around C1 varies more strongly than for the current around C2. The ring current around C1 is largest for **2**, where it stretches to the $C4H_2$ group and in the direction of the center of the C1−C2 bond (compared with that of **1** or **3**). Figures 1b−5b reveal that the contributions of the ring current around C1 to the energy density $\rho^{PSO}(xx)$ largely cancel each other (regions with positive and negative contours are of comparable size). The ring current around C1, in contrast, makes a significant negative contribution to $\rho^{PSO}(xx)$, in line with the fact that the magnetic field of a ring current is strongest in the center of the ring and weak outside the ring.

As discussed above for ethylene (Figure 8), the PSO coupling in *xx* orientation requires an excitation from an occupied orbital with p_y or p_z character at the nucleus into a virtual orbital with p_z or p_y character, respectively. In addition, one of the two orbitals must have p_y character, and the other one must have p_z character at the responding nucleus as well. In a formal single bond, $\rho^{PSO}(xx)$ is dominated by excitations from the σ bond orbital. This orbital has large amplitudes in the regions around both the perturbed and the responding nucleus and, depending on the type of hybridization, 50% or more p character.

The efficiency of the transmission depends mainly on three criteria: (i) The p character of the σ-bond orbital at C1 and C2 should be as high as possible. (ii) Because the bond orbital has p_z character at C1 and C2, the virtual orbital should have p_y character at the bond axis. (iii) Also, it should have a large overlap with the bond orbital and low energy to facilitate the excitation.

TABLE 4: PSO and DSO Orbital Contributions Partitioned into Their Diagonal Terms for the ^1J(C1−C2) Constant of Molecules 1−8[a]

		PSO				DSO			
molecule		isotr.	*xx*	*yy*	*zz*	isotr.	*xx*	*yy*	*zz*
				σ LMO for bond C1−C2					
1		−1.17	−2.55	−0.96	0.00	−0.16	0.17	0.16	−0.81
2		−1.86	−4.50	−1.09	0.00	−0.17	0.18	0.18	−0.86
3		−1.30	−1.95	−1.95	0.00	−0.17	0.17	0.19	−0.88
4		−1.85	−3.63	−1.93	0.00	−0.18	0.20	0.20	−0.93
5		−2.12	−3.18	−3.18	0.00	−0.16	0.22	0.22	−0.91
6		−0.65	−0.97	−0.97	0.00	−0.13	0.20	0.17	−0.71
7		−5.97	−16.58	−1.32	0.00	−0.18	0.27	0.21	−1.02
8		−7.51	−11.27	−11.27	0.00	−0.15	0.25	0.30	−1.07
				π LMO for bond C1−C3					
1		−0.24	−0.43	−0.02	−0.28	0.05	0.04	0.14	−0.03
2		−0.47	−1.16	−0.02	−0.24	0.04	0.04	0.10	−0.04
3		−0.15	0.32	−0.03	−0.73	0.05	−0.02	0.10	−0.01
3		−0.15	−0.03	0.32	−0.73	0.05	0.18	0.12	−0.12
4		−0.33	−0.65	−0.03	−0.32	0.05	0.04	0.11	−0.01
5		−0.36	−0.68	−0.04	−0.38	0.05	0.04	0.13	−0.02
5		−0.36	−0.04	−0.68	−0.38	0.05	0.13	0.04	−0.02
				σ LMO for bond C1−H					
6		−0.10	0.12	−0.02	−0.38	0.05	0.04	0.13	−0.15
6		−0.10	−0.02	0.12	−0.38	0.05	0.16	0.01	0.01
				π LMO for bond C2−C4					
2		−0.33	−0.78	−0.02	−0.19	0.04	0.04	0.10	−0.04
4		−0.28	−0.77	−0.02	−0.04	0.04	0.05	0.11	−0.04
4		0.35	−0.05	2.87	−1.77	0.05	0.10	0.03	0.02
5		0.11	−0.44	−0.03	0.80	0.05	0.04	0.13	−0.02
5		0.11	−0.03	−0.44	0.80	0.05	0.13	0.04	−0.02
				σ LMO for bond C2−H					
1		0.01	0.40	−0.02	−0.33	0.04	0.04	0.09	−0.07
3		−0.15	−0.11	−0.11	−0.23	0.05	−0.02	0.10	−0.04
3		−0.15	−0.11	−0.11	−0.23	0.05	0.08	0.10	−0.04
6		0.17	0.92	−0.02	−0.39	0.05	0.07	0.12	0.00
6		0.17	−0.02	0.92	−0.39	0.05	0.14	0.06	−0.05
				σ LMOs for neighboring bonds at C1					
1	C1−C3	0.00	0.09	0.23	−0.32	0.06	0.11	0.05	0.01
2	C1−C3	−0.02	0.02	0.23	−0.31	0.06	0.12	0.06	0.00
1	C1−H6	−0.07	−0.06	0.26	−0.40	0.05	0.20	0.05	0.08
2	C1−H7	−0.08	−0.10	0.24	−0.36	0.05	0.12	0.05	−0.02
				LMOs for neighboring bonds at C2					
1	C2−H7	0.10	−0.07	0.76	−0.38	0.05	0.12	0.05	−0.02
1	C2−H	0.10	0.12	0.41	−0.23	0.04	0.09	0.07	−0.03
2	C2−C4	−0.07	−0.17	0.41	−0.44	0.06	0.12	0.06	0.00
2	C2−H8	−0.08	−0.25	0.56	−0.55	0.05	0.12	0.05	−0.02

[a] All PSO and DSO contributions are in hertz. SSCC calculations were made at the B3LYP/[7s,6p,2d/4s,2p] level of theory. For atom numbering, see Scheme 1. C2 is the perturbed and C1 is the responding nucleus.

Criterion i favors sp^3-hybridized C atoms over sp^2-hybridized and even more sp-hybridized ones. Criterion ii favors formal single bonds with neighboring π_y bonds over formal single bonds with neighboring pseudo-π bonds. Neighboring π_y bonds imply that there are π_y^* orbitals that, in connection with the σ bonding orbital, can carry ring currents efficiently. This will be true especially if both C1 and C2 are double-bonded (π_y-bonded). In contrast, for C1 and/or C2 being sp^3 hybridized the available pseudo-π_y^* orbitals are less efficient in carrying a PSO current. The largest *xx* value is found in **2**. The σ-bonding orbital of **2** has sp^2 character both at C1 and C2, and both C1 and C2 are π_y-bonded to their neighboring atoms C3 and C4. Consequently, there is a low-lying C1−C2 antibonding π_y^* orbital available.

In **1**, the hybridization of the C1−C2 bonding orbital is higher than that in **2**. However, there is no π_y orbital at C1, and the lowest virtual orbital with π_y character is largely localized at the C1═C3 bond. This explains why the ring current around C1 extends only weakly in the direction of C1−C2. The trend observed in the comparison of **2** and **1** can be extrapolated to reference system **6**. The C1−C2 bond orbital of **6** is indeed sp^3-hybridized at both C1 and C2, which favors the PSO coupling mechanism. However, the low efficiency of the pseudo-π* orbitals in carrying the PSO current results in a small negative contribution of the C1−C2 bonding orbital to PSO(*xx*), which is outweighed by positive contributions from other bonds so that the total value of PSO(*xx*) in **6** is positive.

In both **4** and **5**, π_y^* orbitals of the same character as in **2** are available to carry the induced current. However, the hybridization is sp^2−sp in **4** and sp−sp in **5**, which results in |PSO(*xx*)(**2**)| > |PSO(*xx*)(**4**)| > |PSO(*xx*)(**5**)|. The same trend is seen in the contributions of σ(C1−C2) to *xx* (Table 4). Finally, **3** has both a low hybridization of the C1−C2 bond orbital at C2, viz., sp, and virtual orbitals that are less efficient in carrying an orbital current than those in **4**, **2**, and **5**, which is why **3** has the smallest σ(C1−C2) orbital contribution as well as the smallest PSO(*xx*) value among **1**−**5**.

The excitation from the σ(C1−C2) orbital is the leading contribution to $\rho^{PSO}(xx)$. Only in some particular cases do other occupied orbitals play a significant role. In **4**, because of the angle between the C2−C1 and the C1═C4 bonds, the σ(C1−C3) orbital can conjugate into the virtual π_x orbitals along the C2−C1≡C4 axis. In this orbital, PSO currents can be induced by excitations into a virtual orbital with σ(C1−C2) character. The same holds true for the σ(C2−H6) orbital. The π_y(C2═C3) orbital in **4** can efficiently conjugate into the π_y^*(C1−C4) antibonding orbitals; conversely, π_y(C1≡C4) conjugates into π_y^*(C2═C3). The conjugation effects lead to occupied orbitals that can efficiently mediate a paramagnetic current between C1 and C2. The conjugated occupied orbitals are C1−C2 bonding; the virtual orbitals are C1−C2 antibonding. As a consequence, the induced ring currents around C1 and C2 are equally oriented, with a zero contour between, and the resulting contribution to the SSCC is negative.

The $\rho^{PSO}(yy)$ and $\rho^{PSO}(zz)$ energy densities can be discussed in the same way as the $\rho^{PSO}(xx)$ energy density, which reveals that the former are influenced by a large number of small, and partially contradictory, factors. $\rho^{PSO}(zz)$ is not a useful parameter for describing the nature of the C1−C2 bond because the difference between a $\pi_{x,y} \rightarrow \pi_{y,x}^*$, pseudo-$\pi_{x,y} \rightarrow \pi_{y,x}^*$, $\pi_{x,y} \rightarrow$ pseudo-$\pi_{y,x}^*$, and pseudo-$\pi_{x,y} \rightarrow$ pseudo-$\pi_{y,x}^*$ excitation is larger than the similarity of the orbitals involved suggests. The first leads to a current density and a PSO energy density with a nodal surface through the center of the C−C bond, which implies a large cancellation of positive and negative contributions yielding a positive *zz* value, whereas the other do not lead to such a nodal surface and a compensation of negative and positive contributions. Hence, PSO(*zz*) for **5** is different from the others (0.85 Hz), which in turn cannot be ordered because of the rather different pseudo-π-orbitals participating in **1**, **3**, **2**, and **4**. In addition, this is complicated by the excitation energies, which are involved only indirectly with the nodal pattern of the PSO energy density.

The situation is even more complicated for the *yy* terms, which are also not suitable for a description of the π-bond character of the C1−C2 bond, except that one discusses each bond by itself on the basis of the orbitals involved in the contributing excitations. The *xx* term, however, is more useful because it involves two quantities that influence the bond character. It measures the p character of the σ(C1−C2) orbital and the availability of low-lying π* orbitals. Therefore, we will now discuss the relationship between C1−C2 bond order and the *xx* term as a suitable descriptor of the bond character.

4. Usefulness of the PSO Term for Bond Descriptions

Within the LMO description, the dominating orbital contribution to the isotropic PSO term is given by the σ(C1−C2) orbital rather than the π orbitals. In the same way, *xx* is dominated by the *xx* component of the σ(C1−C2) contribution (Table 4). Both the isotropic and the *xx* orbital contribution depend on the p_σ character of the σ(C1−C2) bond orbital and the availability of π* orbitals where these two factors work in opposite direction. This leads to the quadratic (or cubic) relationship shown in Figure 6 for the total PSO and the NC terms.[24] Similar functional behavior can also be observed if one considers just the PSO and NC terms of the formal single bonds C1−C2 separately, as done in the inset of Figure 6. This leads to the question of whether one has to analyze each major bond type (C−C, C═C, C≡C, aromatic C−C, etc.) by itself.

The PSO(*xx*) component depends on the excitation energies between occupied and virtual orbitals, the overlap between zeroth- and first-order orbitals, and the nodal behavior of the resulting ring currents, which can be derived from the orbital pairs involved in the excitation process. In the case of the excitation energies, one can define an average excitation energy or take just the smallest one to obtain a suitable guess. However, for whatever guess is taken one cannot expect there to be a systematic trend in these parameters, which can be anticipated from π or total bond orders. The latter are properties of the ground state, whereas the excitation energies depend on both ground- and excited-state properties. Similar considerations hold for the overlap between zeroth- and first-order orbitals and their nodal behavior. For example, in the case of **6** there are two pairs of degenerate pseudo-π orbitals and two pairs of degenerate pseudo-π* orbitals, and it is difficult to foresee whether excitations involving these orbitals lead to a nodal surface through the C1−C2 bond in the *zz* current density. (They do not; see above.)

For the purpose of relating the PSO term to ground-state properties such as the bond order, simplifications are necessary: (a) One can divide the virtual orbitals into two groups, π* and pseudo-π* orbitals and classify the occupied σ(C1−C2) orbitals according to the average degree of hybridization $\bar{h}$ at C1 and C2 (i.e., $\bar{h} = 1.5$ for **1**, 2 for **2** and **3**, 1.5 for **4**, 1 for **5**, and 3 for **6**). Any time a pseudo-π orbital is involved, the higher excitation energy is considered by a prefactor $1/a$. (Optimized a values are close to 5.) If a parameter $\bar{h}/a$ is added to the AOM bond order leading to AOM′, then a relationship (Figure 10a) is obtained, which yields for the formal C−C single bond in hyper- or π-conjugated hydrocarbons the right ordering of *xx* terms with AOM′ and suppresses the strong scattering of data points observed when AOM itself is used. However, it is also obvious that hyperconjugated and π-conjugated systems form classes for themselves (Figure 10a) and that AOM′ gives only an indication of how *xx* could be used in a more efficient way to establish the degree of hybridization and π delocalization from magnetic properties. Clearly, *xx* reflects changes in the bond properties due to electron excitation from the ground state to the excited state, which are difficult to verify by calculational means as long as the average excitation energy is not used, and associated with it, an average excited-state geometry (bond order) is defined.

Another way to describe the behavior of the PSO components by ground-state properties is to constrain the analysis to C−C single bonds of the same type of hybridization. By this, the orbital pairs that are predominantly responsible for the orbital currents are largely fixed. In this way, one can relate the PSO components to secondary changes such as a decrease in the excitation energies because of a more dense packing of π orbitals caused by the extension of the conjugated system. Such a change is also reflected by the bond orders; therefore, the PSO components should be directly related to the bond order.

As suitable examples, we have investigated polyenes **2**, **9**, and **10** and polyacetylenes **5**, **11**, and **12** (Scheme 1). The calculated SSCCs ^1J(C−C) and their Ramsey terms are shown in Table 5 together with bond lengths R(C−C) and bond orders NRT and AOM. Simple Hückel theory predicts that with increasing size of the linear polyene (polyacetylene) the π character of the formal single bonds increases and that the central C−C bonds in a polyene (or polyacetylene) have larger π character than the terminal C−C single bonds. This is confirmed by the calculated bond lengths and the AOM bond orders (Table 5). We note that the NRT bond orders systemati-

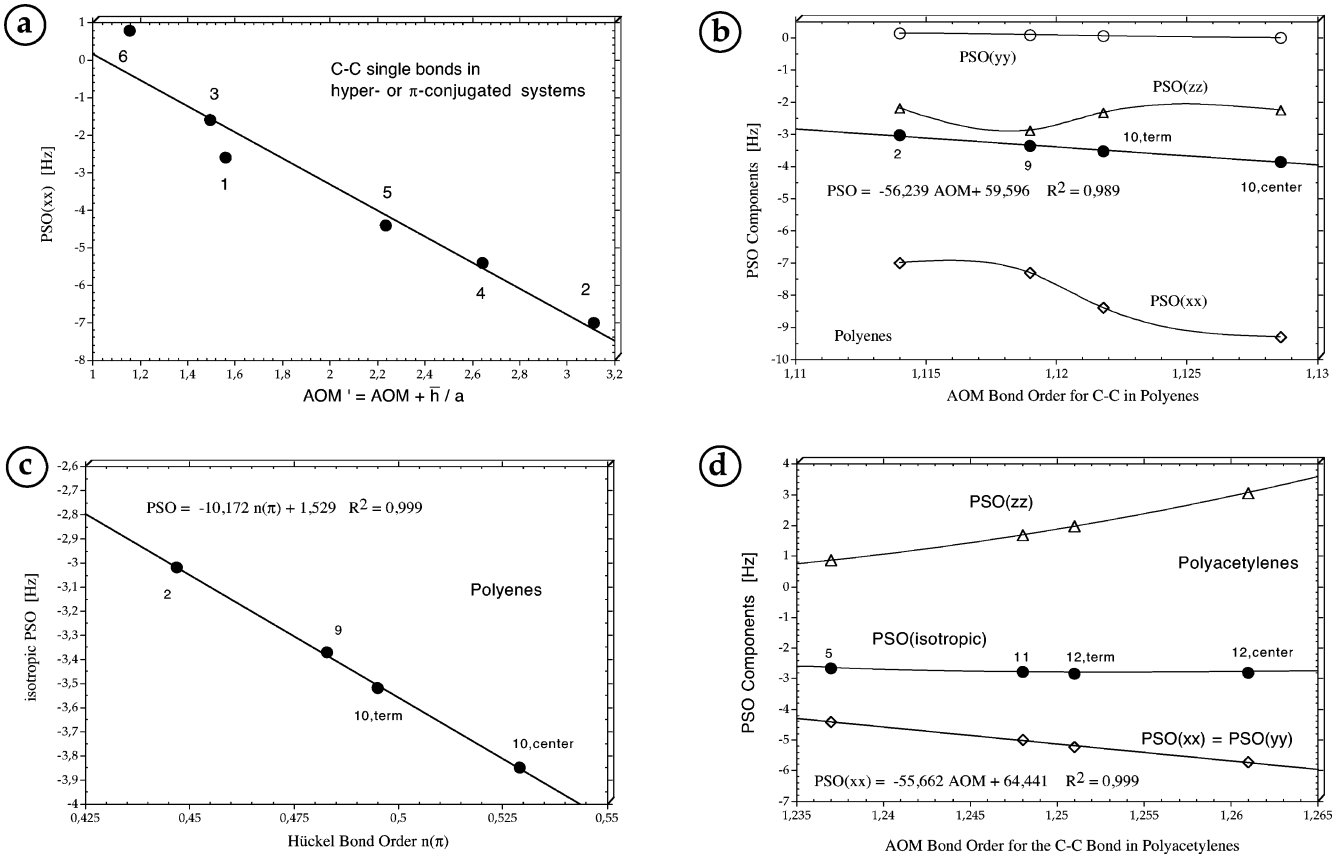

Figure 10. PSO components of ^1J(C−C) as functions of the bond order. (a) PSO(*xx*) as a function of the bond order AOM′, which contains the average hybridization degree $\bar{h}$ and an excitation scaling factor *a* according to AOM′ = AOM + $\bar{h}$/a (see text). (b) PSO components as a function of the AOM bond order in the case of polyenes **2**, **9**, and **10**. (c) Isotropic PSO term as a function of the Hückel π-bond order $n(\pi)$ in the case of polyenes **2**, **9**, and **10**. (d) PSO components as a function of the AOM bond order in the case of polyacetylenes **5**, **11**, and **12**. For numbering of the molecules, see Scheme 1.

TABLE 5: Characterization of the Formal C−C Single Bonds of Some Polyenes and Polyacetylenes by the PSO Components of ^1J(C−C), the Bond Length, and the Bond Order[a]

parameter	2	9	10	10 terminal	5 center	11	12 terminal	12 center
PSO(*xx*)	−7.00	−7.32	−8.40	−9.31	−4.41	−5.01	−0.52	−0.57
PSO(*yy*)	0.15	0.10	0.06	0.01	−4.41	−5.01	−0.52	−0.57
PSO(*zz*)	−2.20	−2.88	−2.33	−2.25	0.85	1.67	0.20	0.31
isotropic PSO	−3.02	−3.37	−3.52	−3.85	−2.66	−2.78	−2.83	−2.80
R(C−C)	1.457	1.446	1.447	1.441	1.369	1.360	1.357	1.348
bond order NRT	1.061	1.072	1.084	1.071	1.115	1.128	1.151	1.122
bond order AOM	1.114	1.119	1.122	1.129	1.237	1.248	1.251	1.261

[a] PSO contributions are in hertz; distance *R*(C−C) is in angstroms. SSCC calculations were made at the B3LYP/[7s,6p,2d/4s,2p] level of theory; geometries and bond orders are at the B3LYP/6-31G(d,p) level of theory. The axis of the C−C single bond is in the *z* direction; the π orbitals are in the *y* direction.

cally fail to indicate the higher bond order of a central C−C bond as compared to the bond order of a peripheral C−C bond in a polyene or polyacetylene. Therefore, the NRT bond orders are not suitable bond descriptors and are no longer considered in this work.

Parts b and d of Figure 10 show that for both polyenes and polyacetylenes the PSO term and its components vary in a regular fashion with the bond order. In the case of the polyenes, the isotropic PSO term turns out to be a better descriptor of the bond than the *xx* component because the former depends linearly on the AOM bond order whereas the latter has a more complicated dependence on the AOM bond order. This is due to the fact that the energies of the σ(C−C) and σ*(C−C) orbitals in a polyene depend on the C−C−C bond angle. This is also true for the in-plane pseudo-π(=CH−CH=) and pseudo-π*-(=CH−CH=) orbitals, which are relevant to the *zz* component. Because the trends in the *xx* and *zz* components are opposite and largely cancel each other and because the *yy* component does not play any significant role (Figure 10b), the linear relationship for the isotropic PSO term results (Figure 10b).

Our motivation to focus on one type of C−C single bond is based on the need to exclude hybridization effects and by this to be able to describe ground- and excited-state properties influencing the PSO components by easily available ground-state properties such as the AOM bond order. The largest changes in the latter are caused by changes in the hybridization of the C atoms connected by a single bond. If these are no longer present, then it should be possible to establish a relationship

between the PSO term and the π-bond order. This is confirmed by the linear relationship between the isotropic PSO term and the Hückel π-bond order for the formal C−C single bond in polyenes shown in Figure 10c. Such a relationship exists for the polyacetylenes for any PSO component because secondary effects resulting from the bending of the carbon chain are excluded; accordingly, all PSO components vary linearly with the AOM and the π-bond order. This also holds for PSO bond-length relationships or when frequencies, force constants, or bond-dissociation energies are correlated with the PSO components.

The linear relationships involving the PSO terms shown in Figure 10 are remarkable because the tiny differences in bond lengths and bond orders lead to relatively strong PSO changes of 1−3 Hz (considering the fact that SSCCs of 0.2 Hz are still measurable nowadays). Of course, the PSO term is not an observable; therefore, it may not be an interesting quantity for the experimentalist. However, the quantum chemical description of bonds differing by just 0.003 and 0.009 Å (see *R* values for 11 and 12 in Table 5) is a difficult task and can lead to misleading results, as demonstrated in this work for the NRT bond orders (Table 5). In this regard, the hypersensitive PSO term is a useful property of the bond, which can be used for a reliable relative comparison of the properties of closely related bonds.

Apart from the special cases considered in Table 5 and Figure 10, the most important result of this work is that the PSO term of a C−C single bond depends on the p character rather than just the π character of the C−C bond. This means that one has to consider both the p_σ and the p_π contributions of the C−C bond. Both can behave in different ways. From **1**−**5**, the p_π character of the C−C single bond increases, whereas the p_σ character is drastically decreased by reduction in hybridization at the C atoms from sp^3 to sp. This has to do with the fact that the PSO term is a quantity that measures the bond both in the ground state and in excited states.

Acknowledgment. Calculations were made on the supercomputers of the Nationellt Superdatorcentrum (NSC), Linköping, Sweden. We thank the NSC for a generous allotment of computer time. J.G. thanks Carl Tryggers Stiftelse for financial support.

Appendix

In this Appendix, the CP-DFT formulation[26] of the Ramsey theory[23] for the indirect nuclear spin−spin coupling constant is briefly summarized. Within CP-DFT, the four Ramsey terms are given as

$$K_{AB}^{DSO} = \frac{2}{3}\sum_{k}^{occ} \langle \phi_K^{(0)} | \mathrm{Tr}\, \underline{\underline{h}}_{AB}^{DSO} | \phi_k^{(0)} \rangle \tag{A1}$$

$$K_{AB}^{PSO} = -\frac{4}{3}\sum_{k}^{occ} \langle \phi_k^{(0)} | \mathbf{h}_A^{PSO} | \vec{\phi}_k^{(B),PSO} \rangle \tag{A2}$$

$$K_{AB}^{FC} = \frac{2}{3}\sum_{k\sigma}^{occ} \langle \psi_{k\sigma}^{(0)} | \mathbf{h}_A^{FC} | \vec{\psi}_{k\sigma}^{(B),FC} \rangle \tag{A3}$$

$$K_{AB}^{SD} = \frac{2}{3}\sum_{k\sigma}^{occ} \langle \psi_{k\sigma}^{(0)} | \mathbf{h}_A^{SD} | \vec{\psi}_{k\sigma}^{(B),SD} \rangle \tag{A4}$$

where the DSO, PSO, FC, and SD operators are defined by eqs A5−A8:

$$\underline{\underline{h}}_{AB}^{DSO} = \left\{\frac{1}{m}\left(\frac{4\pi\epsilon_0\hbar^2}{e^3}\right)^2\right\}\alpha^4\left(\frac{\mathbf{r}_A}{\mathbf{r}_A^3}\cdot\frac{\mathbf{r}_B}{\mathbf{r}_B^3}\underline{\underline{I}} - \frac{\mathbf{r}_A}{\mathbf{r}_A^3}\bigcirc\frac{\mathbf{r}_B}{\mathbf{r}_B^3}\right) \tag{A5}$$

$$\mathbf{h}_A^{PSO} = \left\{\frac{4\pi\epsilon_0\hbar^3}{e^3 m}\right\}\alpha^2\frac{\mathbf{r}_A}{\mathbf{r}_A^3}\times\nabla \tag{A6}$$

$$\mathbf{h}_A^{FC} = \left\{\frac{4\pi\epsilon_0\hbar^3}{e^3 m}\right\}\frac{8\pi}{3}\alpha^2\,\delta(\mathbf{r}_A)s \tag{A7}$$

$$\mathbf{h}_A^{SD} = \left\{\frac{4\pi\epsilon_0\hbar^3}{e^3 m}\right\}\alpha^2\left[3\frac{(\mathbf{s}\cdot\mathbf{r}_A)\mathbf{r}_A}{\mathbf{r}_A^5} - \frac{s}{\mathbf{r}_A^3}\right] \tag{A8}$$

The operators $\mathbf{h}_A^X$ and X = PSO, FC, SD are chosen in such a way that the first-order orbitals become real; this implies that the operators $\mathbf{h}_A^X$ are anti-Hermitian. The position of nucleus N (A or B) is given by vector $\mathbf{R}_N$; $\mathbf{r}_N = \mathbf{r} - \mathbf{R}_N$ gives the distance between an electron and the nucleus, ϵ_0 is the dielectric constant of the vacuum, α is Sommerfeld's fine-structure constant, $\underline{\underline{I}}$ is the unit tensor, and *s* is the electron spin in units of $\hbar$. The prefactors enclosed in braces in eqs A5−A8 are equal to 1 when expressed in atomic units. Note that $\mathbf{h}_A^{PC}$ and $\mathbf{h}_A^{SD}$ are 2 × 2 matrices with respect to the electron spin variables. The symbol ○ denotes the dyadic product of two vectors. The DSO and the PSO parts of the SSCC can be expressed in terms of spin-free orbitals ϕ_k, whereas the FC and the SD parts are given in terms of spin-dependent orbitals ψ_k. Zeroth-order orbitals are denoted by superscript (0), and superscript (B) denotes first-order orbitals resulting from the perturbed nucleus B. The indices of the occupied orbitals will be *k*, *l*, ⋯; those of the virtual orbitals will be *a*, *b*,⋯.

In the first instance, the SSCCs are tensors with respect to the orientations of the perturbed and responding nuclei. (See for example, ref 26.) As molecules in the gas phase or in solution are oriented randomly and rotate rapidly, only the isotropic average of the SSCC, which equals $^1/_3$ of the trace of the corresponding SSCC tensors, is observable.[12,13] Equations A1−A8 give these isotropic average values. For the purpose of investigating the electronic mechanism of spin- spin coupling, the individual components of the SSCCs defined by a given orientation of perturbed and responding nuclei have to be analyzed. One focuses on the diagonal components where the two nuclei are parallel because only the diagonal components contribute to the isotropic average. The diagonal terms of the DSO and PSO parts, for a given orientation *n* of the two nuclei, have the form

$$K_{AB,nn}^{DSO} = 2\sum_{k}^{occ}\langle\phi_k^{(0)}|\,(\mathbf{n}\underline{\underline{h}}_{AB}^{DSO}\mathbf{n})\,|\phi_k^{(0)}\rangle \tag{A9a}$$

$$K_{AB,nn}^{PSO} = -4\sum_{k}^{occ}\langle\phi_k^{(0)}|\left(\mathbf{h}_A^{PSO}\mathbf{n}\right)|\underbrace{\left(\mathbf{n}\vec{\phi}_k^{(B),PSO}\right)}_{=\,|\phi_{k,\mathbf{n}}^{(B),PSO}\rangle}\rangle \tag{A9b}$$

The isotropic coupling constant is then obtained as

$$K_{AB}^{X} = \frac{1}{3}(K_{AB,xx}^{X} + K_{AB,yy}^{X} + K_{AB,zz}^{X}) \tag{A10}$$

The *K* introduced in eqs A1−A8 denotes the reduced SSCC, which describes only the electronic part of the coupling

mechanism and does not reflect gyromagnetic ratios γ_A and γ_B of the coupling nuclei. The measured SSCC is related to J_{AB}

$$J_{AB} = \frac{\gamma_A \gamma_B}{h} K_{AB} \qquad \text{(A11)}$$

where analogous relationships follow for the individual Ramsey terms and their components. In this paper, we present the theory in terms of K for reasons of simplicity but give numerical values for the J to facilitate comparison with experiment.

References and Notes

(1) Pauling, L. *The Nature of the Chemical Bond*; 3rd ed. Cornell University Press: Ithaca, NY, 1960.

(2) (a) *Theoretical Models of Chemical Bonding, Part 2: The Concept of the Chemical Bond*; Maksic, Z. B., Ed; Springer-Verlag: Heidelberg, Germany, 1990. See also (b) McWeeny, R. *Coulsons Chemische Bindung*; Hirzel: Stuttgart, Germany, 1984. (c) Sanderson, R. T. *Chemical Bonds and Bond Energy*; Academic Press: New York, 1976.

(3) See, for example, Gimarc, B. M. *Molecular Structure and Bonding: The Qualitative Molecular Orbital Approach*; Academic Press: New York, 1979.

(4) Coppens, P.; Hall, M. B. *Electron Density Distributions and the Chemical Bond*; Plenum Press: New York, 1981.

(5) (a) Ruedenberg, K. In *Localization and Delocalization in Quantum Chemistry*; Chelvet, O., Daudel, R., Diner, S., Malrieu, J. P., Eds.; D. Reidel Publishing Co: Dordrecht, The Netherlands, 1975; Vol. I, p 223. (b) Ruedenberg, K. *Rev. Mod. Phys.* **1962**, *34*, 326.

(6) (a) Cremer, D.; Kraka, E. *Angew. Chem.* **1984**, *96*, 612. Cremer, D.; Kraka, E. *Angew. Chem., Int. Ed. Engl.* **1984**, *23*, 627. (b) Cremer, D.; Kraka, E. *Croat. Chem. Acta*, **1984**, *57*, 1259.

(7) Kraka, E.; Cremer, D. In *Theoretical Models of Chemical Bonding, Part 2: The Concept of the Chemical Bond*; Maksic, Z. B., Ed.; Springer-Verlag: Heidelberg, Germany, 1990; p 453.

(8) Cremer, D.; Wu, A.; Larsson, J. A.; Kraka, E. *J. Mol. Model.* **2000**, *6*, 396.

(9) Cremer, D.; Larsson, J. A.; Kraka, E. In *Theoretical and Computational Chemistry*; Parkanyi, C., Ed; Elsevier: Amsterdam, 1998; Vol. 5, p 259.

(10) Larsson, J. A.; Cremer, D. *J. Mol. Struct.* **1999**, *485*−*486*, 385.

(11) Cremer, D.; Kraka, E. *J. Am. Chem. Soc.* **1985**, *107*, 3800.

(12) See, for example, *Encyclopedia of Nuclear Magnetic Resonance*; Grant, D. M., Harris, R. K., Eds; Wiley: Chichester, U.K., 1996; Vol 1−8.

(13) (a) Pople, J. A.; Schneider, W. G.; Bernstein, H. J. *High-Resolution Nuclear Magnetic Resonance*; McGraw-Hill: New York, 1959. (b) Emsley, J. W.; Feeney, J.; Sutcliffe, L. H. *High-Resolution Nuclear Magnetic Resonance Spectroscopy*; Pergamon: Oxford, U.K., 1966.

(14) Muller, N.; Pritchard, D. E. *J. Chem. Phys.* **1959**, *31*, 768.

(15) Newton, M. D.; Schulman, J. M.; Manus, M. M. *J. Am. Chem. Soc.* **1974**, *96*, 17.

(16) Lynden-Bell, R. M.; Sheppard, N. *Proc. R. Soc. London, Ser. A* **1962**, *269*, 385.

(17) (a) Frei, K.; Bernstein, H. J. *J. Chem. Phys.* **1963**, *38*, 1216. (b) Günther, H.; Herrig, W. *Chem. Ber.* **1973**, *106*, 3938.

(18) Kalinowski, H. O.; Berger, S.; Braun, S. *^{13}C NMR-Spektroskopie*; Thieme: New York, 1984, and references therein.

(19) Günther, H. *NMR-Spectroscopy*; Thieme: New York, 1983.

(20) Kamienska-Trela, K. *Spectrochim. Acta, Part A* **1980**, *36*, 239.

(21) Wardeiner, J.; Lüttke, W.; Bergholz, R.; Machinek, R. *Angew. Chem., Int. Ed. Engl.* **1982**, *21*, 872.

(22) For a review on hybrid orbitals, see Bingel, W. A.; Lüttke, W. *Angew. Chem.* **1981**, *93*, 944. Bingel, W. A.; Lüttke, W. *Angew. Chem., Int. Ed. Engl.* **1981**, *20*, 899.

(23) Ramsey, N. F. *Phys. Rev.* **1953**, *91*, 303.

(24) Cremer, D.; Kraka, E.; Wu, A.; Lüttke, W. *Chem. Phys. Phys. Chem.*, in press, 2004.

(25) Gräfenstein, J.; Cremer, D. *Chem. Phys. Lett.* **2004**, *383*, 332.

(26) Sychrovský, V.; Gräfenstein, J.; Cremer, D. *J. Chem. Phys.* **2000**, *113*, 3530.

(27) For related work, see (a) Helgaker, T.; Watson, M.; Handy, N. C. *J. Chem. Phys.* **2000**, *113*, 9402. (b) Barone, V.; Peralta, J. E.; Contreras, R. H.; Snyder, J. P. *J. Phys. Chem. A* **2002**, *23*, 5607. (c) Contreras, R. H.: Peralta, J. E.; Giribet, C. G.; de Azua, M. C.; Facelli, J. C. *Annu. Rep. NMR Spectrosc.* **2000**, *41*, 55. (d) Peralta, J. E.; Barone, V.; de Azua, M. C.; Contreras, R. H. *Mol. Phys.* **2001**, *99*, 655. (e) Peralta, J. E.; de Azua, M. C.; Contreras, R. H. *Theor. Chem. Acc.* **2000**, *105*, 165.

(28) Wu, A.; Gräfenstein, J.; Cremer, D. *J. Phys. Chem. A* **2003**, *107*, 7043.

(29) Gräfenstein, J.; Tuttle, T.; Cremer, D. *J. Am. Chem. Soc.*, submitted for publication.

(30) Wu, A.; Cremer, D. *Phys. Chem. Chem. Phys.* **2003**, *5*, 4541.

(31) Gräfenstein, J.; Cremer, D. *Chem. Phys. Lett.* **2004**, *387*, 415.

(32) Becke, A. D. *J. Chem. Phys.* **1993**, *98*, 5648.

(33) Lee, C.; Yang, W.; Parr, R. *Phys. Rev. B* **1988**, *37*, 785.

(34) Huzinaga, S. *Approximate Atomic Wave Functions*; University of Alberta: Edmonton AB, Canada, 1971.

(35) Kutzelnigg, W.; Fleischer, U.; Schindler, M. *NMR*: *Basic Principles and Progress*; Springer: Heidelberg, Germany, 1990; Vol. 23, p 165.

(36) Hirota, E.; Matsumara, K.; Imachi, M.; Fujio, M.; Tsuno, Y. *J. Chem. Phys.* **1977**, *66*, 2660.

(37) Allena, H. C.; Plyler, E. K. *J. Am. Chem. Soc.* **1958**, *80*, 2673.

(38) Baldacci, A.; Ghersetti, S.; Hurlock, S. C.; Rao, K. N. *J. Mol. Spectrosc.* **1976**, *39*, 116.

(39) Boys, S. F. *Rev. Mod. Phys.* **1960**, *32*, 296.

(40) Cioslowski, J.; Mixon, S. T. *J. Am. Chem. Soc.* **1991**, *113*, 4142.

(41) Bader, F. R. W. *Atoms in Molecules: A Quantum Theory*; International Series of Monographs on Chemistry, no. 22; Clarendon Press: Oxford, U.K., 1995.

(42) (a) Carpenter, J. E.; Weinhold, F. *J. Mol. Struct.: THEOCHEM* **1988**, *46*, 41. (b) Reed, A. E.; Weinstock, R. B.; Weinhold, F. *J. Chem. Phys.* **1985**, *83*, 735. (c) Reed, A. E.; Curtiss, L. A.; Weinhold, F. *Chem. Rev.* **1988**, *88*, 899.

(43) (a) Glendening, E. D.; Weinhold, F. *J. Comput. Chem.* **1998**, *19*, 593. (b) Glendening, E. D.; Weinhold, F. *J. Comput. Chem.* **1998**, *19*, 610. (c) Glendening, E. D.; Badenhoop, J. K.; Weinhold, F. *J. Comput. Chem.* **1998**, *19*, 628.

(44) Kraka, E.; Gräfenstein, J.; Filatov, M.; He, Y.; Gauss, J.; Wu, A.; Polo, V.; Olsson, L.; Konkoli, Z.; He, Z.; Cremer, D. *COLOGNE2003*; Göteborg University: Göteborg, Sweden, 2003.

(45) Frisch, M. J.; Trucks, G. W.; Schlegel, H. B.; Scuseria, G. E.; Robb, M. A.; Cheeseman, J. R.; Zakrzewski, V. G.; Montgomery, J. A., Jr.; Stratmann, R. E.; Burant, J. C.; Dapprich, S.; Millam, J. M.; Daniels, A. D.; Kudin, K. N.; Strain, M. C.; Farkas, O.; Tomasi, J.; Barone, V.; Cossi, M.; Cammi, R.; Mennucci, B.; Pomelli, C.; Adamo, C.; Clifford, S.; Ochterski, J.; Petersson, G. A.; Ayala, P. Y.; Cui, Q.; Morokuma, K.; Malick, D. K.; Rabuck, A. D.; Raghavachari, K.; Foresman, J. B.; Cioslowski, J.; Ortiz, J. V.; Stefanov, B. B.; Liu, G.; Liashenko, A.; Piskorz, P.; Komaromi, I.; Gomperts, R.; Martin, R. L.; Fox, D. J.; Keith, T.; Al-Laham, M. A.; Peng, C. Y.; Nanayakkara, A.; Gonzalez, C.; Challacombe, M.; Gill, P. M. W.; Johnson, B. G.; Chen, W.; Wong, M. W.; Andres, J. L.; Head-Gordon, M.; Replogle, E. S.; Pople, J. A. *Gaussian 98*, revision A.9; Gaussian, Inc.: Pittsburgh, PA, 1998.

(46) Kaski, J.; Lantto, P.; Vaara, J.; Jokisaari, J. *J. Am. Chem. Soc.* **1998**, *120*, 3993.

(47) Ruden, A. T.; Lutnæs, O. B.; Helgaker, T.; Ruud, K. *J. Chem. Phys.* **2003**, *118*, 9572 and references therein.

(48) Jackowski, K.; Wilczek, M.; Pecul, M.; Sadlej, J. *J. Phys. Chem. A* **2000**, *104*, 5955, 9806.

(49) (a) Polo, V.; Kraka, E.; Cremer, D. *Mol. Phys.* **2002**, *100*, 1771. (b) Polo, V.; Kraka, E.; Cremer, D. *Theor. Chem. Acc.* **2002**, *107*, 291. (c) Polo, V.; Gräfenstein, J.; Kraka, E.; Cremer, D. *Chem. Phys. Lett.* **2002**, *352*, 469. (d) Polo, V.; Gräfenstein, J.; Kraka, E.; Cremer, D. *Theor. Chem. Acc.* **2003**, *109*, 22.

(50) Bauernschmitt, R.; Ahlrichs, R. *J. Chem. Phys.* **1996**, *104*, 9047.